Fluorine-19 NMR of Solids Containing Both Fluorine and Hydrogen

Shinji Ando, Robin K. Harris & Ulrich Scheler

Volume 9, pp 531–550

in

Encyclopedia of Nuclear Magnetic Resonance
Volume 9: Advances in NMR
(ISBN 0471 49082 2)

Edited by

David M. Grant and Robin K. Harris

Fluorine-19 NMR of Solids Containing Both Fluorine and Hydrogen

Shinji Ando

Department of Organic and Polymeric Materials, Tokyo Institute of Technology, Okayama, Tokyo, Japan

Robin K. Harris

Department of Chemistry, University of Durham, South Road, Durham, UK

&

Ulrich Scheler

Institut für Polymerforschung e.V., Dresden, Germany

1	Introduction: Special Problems	1
2	Special Techniques and Experimental Requirements	2
3	Cross Polarization Dynamics between ^{1}H and ^{19}F	4
4	Fluoropolymers	9
5	Fluorinated Organic Compounds	13
6	Fluorinated Organometallic and Metal Coordination Compounds	18
7	Fluorinated Inorganic Compounds	18
8	Concluding Remarks	18
9	References	19

1 INTRODUCTION: SPECIAL PROBLEMS

Since the early days of NMR, ^{19}F has been recognized as one of the most useful nuclei, and it has been widely studied for liquids and solutions. This is because it is present in 100% natural abundance, has a relatively high resonance frequency (near to that of the proton), and has a spin quantum number of 1/2. These properties convey very favorable sensitivity in the NMR experiment – the receptivity is 83.4% of that for ^{1}H and 4.90×10^{3} of that for ^{13}C. Moreover, the chemical shift range for ^{19}F is comparable to that of, say, ^{13}C and well over an order of magnitude greater than that for ^{1}H. It follows that, of the obvious nuclei used to examine fluorinated systems containing hydrogen by NMR, fluorine will often be preferred. However, although there have been a number of reports of ^{19}F relaxation parameters and broadline spectra of solids containing fluorine, the use of high-resolution ^{19}F spectra for studying such systems has been relatively limited. Indeed, until relatively recently the total amount of high-resolution ^{19}F NMR work on solids of all types was surprisingly small. It has been reviewed twice in the past decade.[1,2] This lack of reported work is particularly marked for systems containing both fluorine and hydrogen, which form the special topic of this article.

Paradoxically, the reasons for the relative lack of activity on ^{19}F are two of the major advantages of the nucleus, namely the 100% natural abundance and its high magnetic moment. These imply that dipolar interactions (both homonuclear and heteronuclear) are likely to be very strong. The present review will be largely limited to (^{19}F, ^{1}H) double resonance studies, usually involving ^{19}F magic-angle spinning (MAS) spectra obtained with proton decoupling. Associated relaxation time measurements, some related static experiments and some very-high speed MAS investigations will also be covered. Such experiments give improved quality of spectra for both static and magic-angle spinning experiments (especially yielding higher resolution for the latter), and also simplify the interpretation of relaxation data. Also, additional experiments become feasible from the $^{1}H \rightarrow {}^{19}F$ cross-polarization operation. However, the excitation bandwidth required for ^{19}F spectra, especially for high-field spectrometers, is a further source of experimental problems – for example, at 11 T, 100 ppm, which is insufficient for most spectra, is the equivalent of 47 kHz.

All the early ^{19}F NMR work on solid fluorinated systems that also contain hydrogen involved measurements of ^{19}F relaxation and broadline spectra, using what are now thought of as 'classical' NMR techniques.[3,4] Since proton decoupling was not generally employed, there are in principle complications in treating the experimental data which arise from cross-relaxation between ^{19}F and ^{1}H. This problem renders simple T_1 measurements (e.g., by inversion-recovery) intrinsically not single-exponential and raises questions about the influence of the nuclear Overhauser effect. Such issues were generally ignored in the early literature in this area, though they have been addressed by some authors.[5] Of course, all the relevant work before the advent[6] of the combined CPMAS suite of techniques in 1976 was based on low-resolution experiments. The data were interpreted in terms of dipolar interactions rather than chemical shifts and gave information on molecular-level mobility (and domain structure in polymers) rather than chemical structure.

However, there was a long delay following the development of CPMAS NMR before the new techniques were significantly employed for solid fluorinated materials which also contained hydrogen. This is because (^{19}F, ^{1}H) double-resonance experiments are significantly more difficult than analogous (^{13}C, ^{1}H) work, which is a result of the proximity of the resonance frequencies of ^{19}F and ^{1}H (within 6%). Since, for work on solids, decoupling protons from fluorines requires very high powers, there are obvious problems involving the efficiency of r.f. filtering, which inhibited developments. Moreover, without such filtering, $^{1}H \rightarrow {}^{19}F$ cross polarization is not feasible, thus preventing a wide range of informative experiments from taking place. However, the NMR community was in general, perhaps, too timid in this matter, since the first commercial $^{19}F-\{^{1}H\}$ probes suitable for solids were found to be very effective.[7–11] Recently, it has been shown (see below) that very-high-speed MAS is often an acceptable alternative to $^{19}F-\{^{1}H\}$ decoupling in moderate-speed MAS work.

Even with efficient ^{1}H decoupling, achieving high-resolution ^{19}F spectra of polyfluorinated systems presents difficulties because of the strong (^{19}F, ^{19}F) dipolar interactions, which require either multipulse homonuclear decoupling pulse

sequences (e.g., MREV 8) combined with modest-speed MAS (CRAMPS) or very fast (>20 kHz) MAS for their effective removal. Early work on both methods[12,13] was directed at perfluorinated systems. The technical difficulties involved meant that there was only very limited use of these techniques for hydrogen-fluorine systems until the mid-1990s. The next section will show how the experimental situation has now dramatically changed.

2 SPECIAL TECHNIQUES AND EXPERIMENTAL REQUIREMENTS

The origin of the attraction of ^{19}F as a probe nucleus for NMR also results in the majority of the experimental difficulties. Both the dipolar coupling and the chemical shift anisotropy are first-order anisotropic interactions, which are most conveniently averaged by magic-angle sample spinning (MAS). However, when spinning speeds are modest (<20 kHz), as has always been the case until very recently, it is also essential to effectively eliminate the influence of H,F dipolar coupling (for chemical systems containing both nuclei) by the usual heteronuclear double-resonance techniques. However, in the early days of high-resolution solid-state NMR this was thought to be a difficulty (see below) so that substantial work in this area only started in about 1992. In more recent years, the development of high-speed MAS systems, allowing for spinning speeds in excess of 30 kHz, has rendered the acquisition of high-resolution solid-state ^{19}F NMR spectra of compounds containing both abundant protons and fluorines possible without proton decoupling.[13–15]

However, MAS provides the same degree of line narrowing throughout the entire experiment, which is somewhat contrary to one of the major advantages of NMR, the possibility to manipulate and separate interactions. Therefore, even under high-speed MAS double-resonance experiments are desirable. Although proton decoupling leads to no significant resolution enhancement at such high speeds (though splittings arising from H,F isotropic indirect coupling are eliminated, resulting in some improvement), there is a general need for double-resonance experiments to manipulate the heteronuclear dipolar coupling for certain periods of the experiment. The application of high-speed (>20 kHz) MAS requires dedicated equipment that might not always be available. The low-volume rotors present possible difficulties for sample handling. For receptivity the small volume is not usually a problem (except for 'dilute' fluorine cases, such as compounds at interfaces), because the narrow lines from high-speed MAS result in good apparent signal-to-noise ratio. On the other hand, the small sample volume required in the high-speed MAS systems can be an advantage, when novel compounds, only obtainable in very small quantities, are investigated. The major advantage in the application of fast MAS, however, is the simultaneous averaging of the homonuclear fluorine–fluorine coupling, which can be strong in fluorine-rich systems (Figure 1). To follow the time development of any process (such as relaxation) in the experiment, rotor-synchronous detection is usually applied to exclude from the data analysis the additional time-dependence resulting from MAS.

The classical spectrometer design, based on an X channel, together with a proton channel mostly used for decoupling,

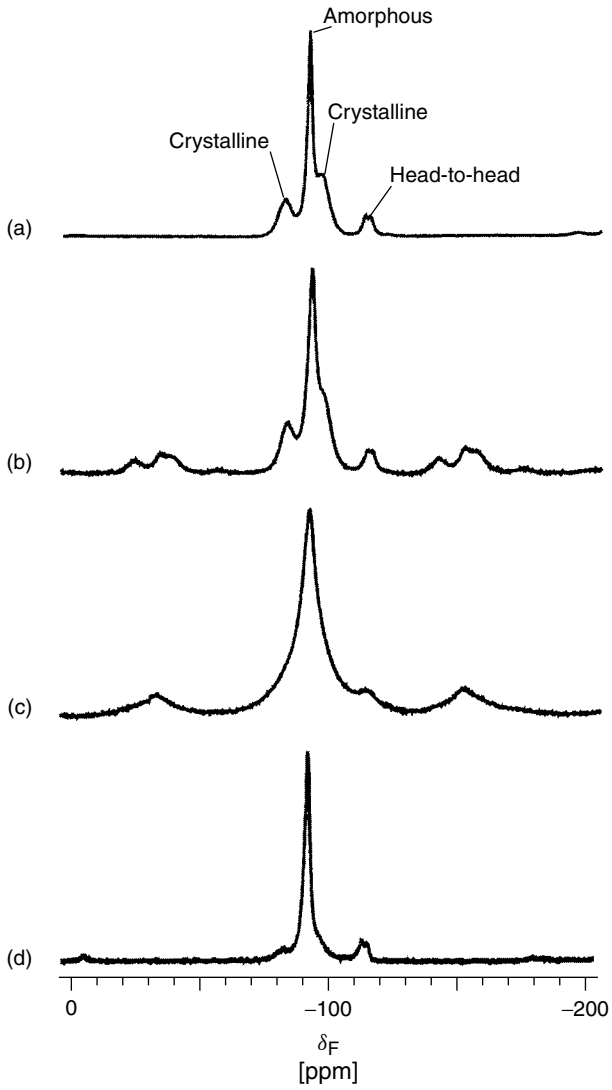

Figure 1 282 MHz fluorine-19 MAS NMR spectra of PVDF: (a) 32 kHz spin rate with no proton decoupling; (b) 16 kHz spin rate with proton decoupling; (c) 16 kHz spin rate with no proton decoupling; and (d) REDOR spectrum (mixing time 0.4 ms; 10 rotor cycles) with 32 kHz spin rate and proton decoupling

is inappropriate for proton–fluorine double-resonance experiments. Because the magnetogyric ratios of almost all X nuclei are lower than that of the proton by at least a factor of 0.4, the frequency range in the X channel of traditional spectrometers is limited. A flexible second channel is therefore needed for proton–fluorine double resonance. The same is true for the probe-head, since a typical H–X solid-state probe-head is based on a relatively large frequency separation. Usually, there is a high-frequency channel tunable to proton and fluorine, with an X channel that is also narrow-band but can be tuned to a wide range of frequencies. The separation/decoupling between the two RF channels is based on the large difference of the resonance frequencies of H and X.

The Larmor frequencies of proton and fluorine nuclei are separated by only 6%. Therefore, the standard double-resonance probe design is not applicable, so that a dedicated probe-head is required for proton–fluorine double resonance. The first reported proton-decoupled fluorine solid-state NMR

spectra were obtained[8–11,16] using dedicated double-resonance probes. Such probes are based on traditional technology, with oscillators and transmission lines. They are specially made for the two frequencies and do not allow more extended tuning. Another option is the use of an overcoupling network, introduced by Maas et al.[17] An additional oscillator inserted between the transmitter and the probe splits the high-frequency resonance of a traditional double-resonance probe symmetrically into two. While this setup was originally developed to achieve simultaneous proton and fluorine decoupling for ^{13}C-observe operation, it can also be applied for proton–fluorine double-resonance experiments. Appropriate external filtering also has to be employed. External RF filters are in any case needed to achieve the attenuation of more than 60 dB between the two channels that is necessary for the acquisition of any spectrum under high-power decoupling. Because the ^{19}F and ^{1}H frequencies are so close, filters of extremely narrow bandwidth have to be used. These filters may influence the rise and fall times of pulses.

The only known applications[18,19] of proton–fluorine double-resonance experiments where no bandpass filters were in use are multiple-pulse experiments. In those experiments no decoupling pulse is present during data acquisition. Omitting external RF filters allows shorter pulses, because there is no bandwidth limitation and no insertion loss. The usual multipulse sequences such as WAHUHA, MREV8 or BR24 are designed to average homonuclear dipolar coupling, which is bilinear in the spin operators. As a side effect they scale both the chemical shift and the heteronuclear dipolar coupling, which are each linear in the spin operators. Strong heteronuclear dipolar coupling (e.g., the coupling between protons and fluorine nuclei) results in an unacceptable linewidth. Therefore, heteronuclear decoupling has to be included, which is achieved by π pulses on the non-detected channel, synchronized with the multipulse sequence on the detection channel (Figure 2).

A minor additional problem appears in solid-state NMR probes dedicated to proton–fluorine double-resonance NMR: the question of probe background signals. Especially when variable-temperature experiments are required, there is little possibility to avoid both proton and fluorine-containing materials in capacitors and all structural materials in the sensitive part of the probe simultaneously. Therefore, usually one or the other has to be selected when designing/manufacturing the probe. Generally the acquisition of fluorine spectra is more desirable than that of proton spectra because of the information content in the larger chemical range of the former. However, in proton-detected experiments a background signal will then be present. The small chemical shift range of protons, however, permits detection at a small spectral width, where background signals from static solid material only show up as a minor baseline distortion.

Various experiments for background suppression have been proposed, such as composite pulses.[20] Another possibility is the excitation of fluorine magnetization via proton–fluorine cross polarization. Materials used in NMR probe manufacturing are usually perfluorinated and do not generate a ^{19}F signal from $^{1}\text{H} \rightarrow {}^{19}\text{F}$ CP. Similarly, background-free ^{1}H spectra can be obtained by $^{19}\text{F} \rightarrow {}^{1}\text{H}$ CP. However, both methods for background suppression introduce additional uncertainties for the experiment and usually inhibit quantitative analysis of the spectra, though they also allow additional useful measurements to be made. The preferable way is just to avoid the probe background signal for the experiment desired.

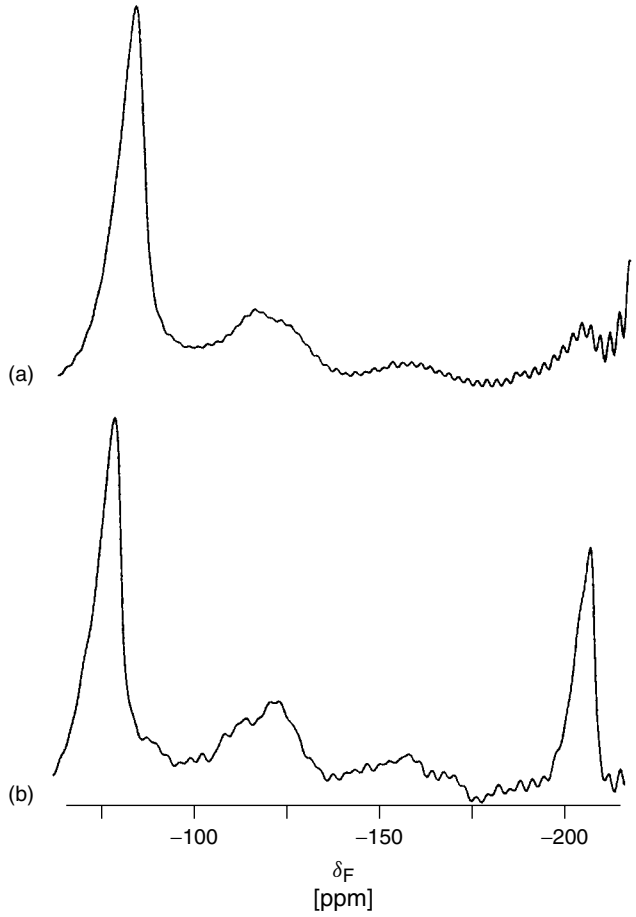

Figure 2 Combined rotational and multipulse experiments on a semifluorinated tetrapropyl-adamantane at 188.29 MHz: ^{19}F CRAMPS with synchronized pulses on the proton channel

Of course, most of the pulse sequences used traditionally for $^{1}\text{H} \rightarrow {}^{13}\text{C}$ CPMAS NMR (such as dipolar dephasing and two-dimensional HETCOR/EXSY) can be adapted to acquire $^{1}\text{H} \rightarrow {}^{19}\text{F}$ CPMAS spectra, starting with the simple CP sequence (Figure 3a). For instance, the WISE sequence[21] (Figure 3b) can be used[22] to obtain ^{1}H bandshapes with the chemical shift discrimination inherent in the ^{19}F spectrum. Usually the homonuclear F,F coupling requires fast MAS for resolution in the ^{19}F spectrum. Therefore, the ^{1}H band breaks up into spinning sidebands (ssb). The second moment of the ssb manifold contains valuable information on the residual dipolar coupling and can be used as a measure of mobility.[23] Moreover, various techniques can be applied[24,25] to discriminate between well-resolved ^{19}F subspectra of different domains in heterogeneous solids, such as use of a ^{1}H spin-lock ($T_{1\rho}^{H}$) or ^{1}H inversion recovery or T_2^H decay (delayed contact) prior to CP (Figure 3c). Similarly, a post-CP ^{19}F spin-lock ($T_{1\rho}^{F}$) or T_2^F decay (delayed acquisition) can be used, as can a one-dimensional (fixed mixing time) REDOR sequence, radiofrequency-driven recoupling (RFDR), a dipolar filter, or DIVAM.[26] The result of a REDOR selection for the amorphous region of the ^{19}F spectrum of poly(vinylidene fluoride), PVDF,

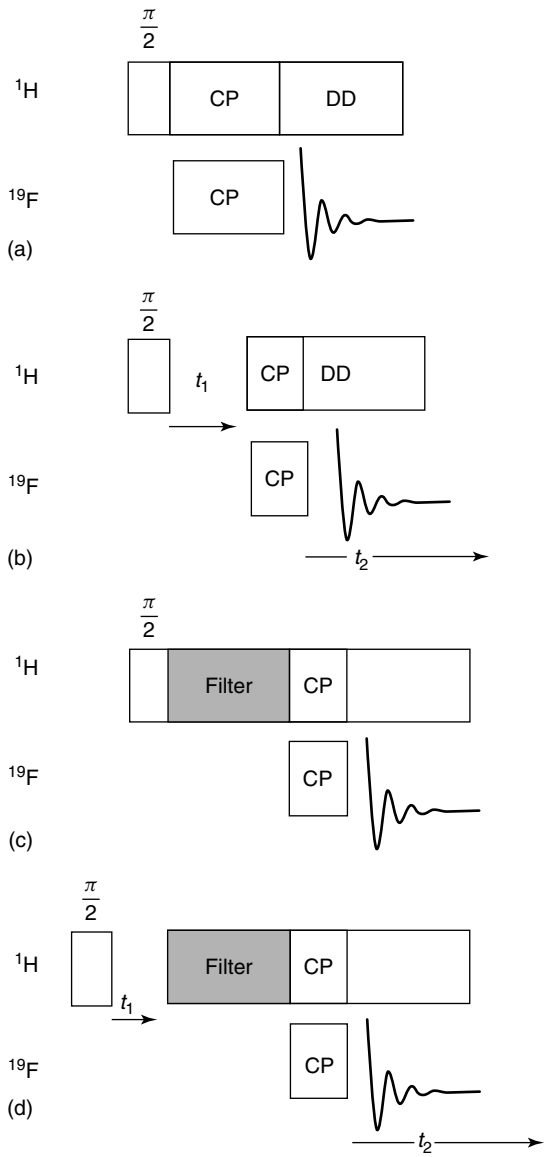

Figure 3 Pulse sequences used for proton–fluorine double-resonance experiments: (a) cross polarization; (b) wideline separation; (c) cross polarization after selection of a sub-ensemble of the proton spins based on proton relaxation times. Possible filters are: dipolar filter, $T_{1\rho}^{H}$ filter, T_{1}^{H} filter; (d) WISE experiment for a sub-ensemble after selection by a magnetization filter

is shown in Figure 1(d). Of course, the simple CPMAS sequence with variable contact time is itself discriminatory, especially when compared to single-pulse excitation (SPE) with MAS. Spin-diffusion can be studied[27] using the Goldman-Shen[28] type of sequence, with appropriate filtering, and the WISE experiment can be combined with various filtering arrangements (Figure 3d). The results of a number of filtering experiments on polymer spectra are discussed in Section 4.

Besides the thermodynamic analysis of the cross polarization dynamics for multiple spin baths, which will be described in the following section, there is the possibility to break the complicated multi-spin system experimentally into a superposition of spin pairs without diluting the sample. This idea makes use of the fact that in a spin-pair under cross polarization the magnetization oscillates between the two coupled spins (dipolar oscillation),[26,29,30] which has been reported for rare cases. However, usually such isolated spin pairs are not present in the sample and the dipolar oscillations are smeared out because the homonuclear dipolar coupling results in spin diffusion. The dipolar oscillations are often ignored for the thermodynamic treatment of the cross-polarization experiment.

Under a spin lock at the magic angle (Lee–Goldburg experiment) the homonuclear dipolar coupling is readily suppressed.[31] The heteronuclear dipolar coupling can be retained when simultaneously applying spin-lock fields at both frequencies to fulfil the Hartmann–Hahn condition.[32] The inherent beauty of this technique lies in the fact that a complex network of dipolar couplings can be broken down to a superposition of pairwise couplings, which are easily interpreted. While this approach has been applied to a case of proton-carbon cross polarization,[33] preliminary studies of proton–fluorine Lee–Goldburg cross polarization have been reported.[34] The complication here is that the homonuclear coupling in both spin baths has to be suppressed. This requires the application of spin-locking at the magic angle on both channels, resulting in a magnetization oriented at the magic angle (which requires an additional read-out pulse). The experiments can be simplified again under fast MAS, where the lines in the fluorine spectrum are well separated anyway. Because the homonuclear coupling is scaled by a factor of (-2) under the spin lock, this appears to be sufficient in many cases. For an example (5-fluoro-2 trifluorobenzoic acid), the signals for the CF and the CF_3 fluorines are well-resolved under MAS.[35] For each fluorine site the internuclear distances to the various neighboring protons have been determined. When the matching is on the first spinning sideband of the Hartmann–Hahn condition, the detected coupling (and thus the distance) is independent of the sample spinning frequency. Because the easiest data evaluation is performed from rotor-synchronized detection, the range of dipolar couplings is limited, so that the maximum coupling that can be characterized is determined by the spinning speed. The distances determined using this approach correspond within experimental error to those obtained from structural molecular simulations.

3 CROSS POLARIZATION DYNAMICS BETWEEN ^{1}H AND ^{19}F

A phenomenological spin thermodynamics[36–39] theory based on the spin-temperature hypothesis has been employed[39,40] to analyze the cross polarization (CP) dynamics between fluorine and proton in solids. The inverse spin temperature β, which is defined as $\hbar/kT$, is proportional to the magnitude of magnetization in the case that only the Zeeman interaction is considered. The variations with time of the inverse spin temperatures, β_H and β_F for the H and F spin baths, are described within this framework. The two spin baths can be in contact with each other and coupled with the lattice, which is suggested to have an infinitely high heat capacity at β_L as depicted in Figure 4.

The rate of the polarization transfer from H to F spin baths is characterized by a time constant T_{HF}. Under the spin-lock condition in the presence of simultaneous rf fields of B_{1F} for F and B_{1H} for H, each link between a spin bath

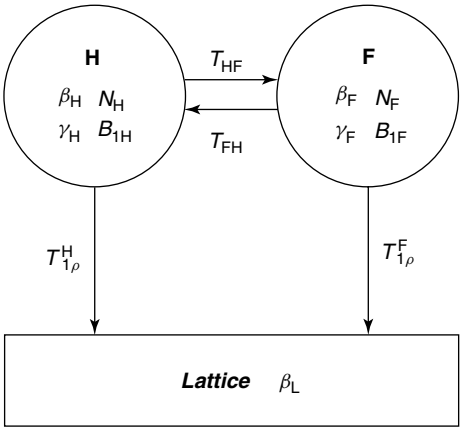

Figure 4 Schematic representation of an abundant ^{1}H spin bath and an abundant ^{19}F spin bath, which are spin-locked by RF irradiation and coupled to the lattice as expressed by their spin-lattice relaxation times in the rotating frame, $T^H_{1\rho}$ and $T^F_{1\rho}$ respectively. The rates of polarization transfer between the two spin baths are represented by the cross-relaxation times T_{HF} (H → F) and T_{FH} (F → H). β is the inverse spin temperature, N the density of spins, γ the gyromagnetic ratio, and B_1 the RF field for spin locking

and the lattice is characterized by a spin-lattice relaxation time in the rotating frame, $T^F_{1\rho}$ for F and $T^H_{1\rho}$ for H. When there is a difference between β_F and β_H, polarization transfer occurs between H and F spins during the contact time (t_{CP}) of cross-polarization (CP) and TORQUE[41] experiments. We assume that β in each spin bath is immediately equilibrated. Hence, oscillation of magnetization between H and F spins is neglected. Such phenomena can occur when there are strongly coupled H–F spin pairs. In addition, we consider only experimental situations where magic-angle spinning does not interfere with the CP process.

Assuming first-order kinetics, the variations of β_F and β_H under a cross-relaxation condition can be described by the coupled differential equations,

$$\frac{d}{dt}\beta_F = -\frac{1}{T_{HF}}(\beta_F - \beta_H) - \frac{1}{T^F_{1\rho}}\beta_F$$
$$\frac{d}{dt}\beta_H = -\frac{\varepsilon}{T_{HF}}(\beta_H - \beta_F) - \frac{1}{T^H_{1\rho}}\beta_H \quad (1)$$

where ε is defined as

$$\varepsilon = \frac{N_F(\gamma_F B_{1F})^2}{N_H(\gamma_H B_{1H})^2} \quad (2)$$

The N and the γ are the number of spins and the gyromagnetic ratio for the indicated nuclear type, respectively. When the Hartmann–Hahn condition

$$\gamma_H B_{1H} = \gamma_F B_{1F} \quad (3)$$

is achieved, ε is equal to N_F/N_H. In the case of H → F cross polarization, equation (1) can be straightforwardly solved under the initial conditions ($t_{CP} = 0$):

$$\beta_F = 0 \text{ and } \beta_H = \beta_{H0} \quad (4)$$

The dependence of β_F on t_{CP}, which corresponds to an evolution of F magnetization as a function of contact time in the standard CP experiment (which we will refer to as a CP curve), can be expressed as follows:

$$\left[\frac{\beta_F(t)}{\beta_{H0}}\right]_{CP} = \frac{1}{a_+ - a_-} \times \left[-\exp\left(-\frac{a_+}{T_{HF}}t_{CP}\right) + \exp\left(-\frac{a_-}{T_{HF}}t_{CP}\right)\right] \quad (5)$$

where
$$a_\pm = a_0 \pm \sqrt{a_0^2 - b} \quad (6)$$

with
$$a_0 = \frac{1}{2}\left(1 + \varepsilon + \frac{T_{HF}}{T^H_{1\rho}} + \frac{T_{HF}}{T^F_{1\rho}}\right) \quad (7)$$

and
$$b = \frac{T_{HF}}{T^H_{1\rho}}\left(1 + \frac{T_{HF}}{T^F_{1\rho}}\right) + \varepsilon\frac{T_{HF}}{T^F_{1\rho}} \quad (8)$$

In the same way, the dependence of β_F on t_{CP} in the H → F TORQUE experiments (which we will refer to as a TORQUE curve) can be expressed as

$$\left[\frac{\beta_F(t)}{\beta_{H0}}\right]_{TOR} = \exp\left(-\frac{t_{SL}}{T^H_{1\rho}}\right)\left[\frac{\beta_F(t)}{\beta_{H0}}\right]_{CP} \quad (9)$$

where t_{SL} is a spin-lock time for the H nuclei prior to the cross polarization to F nuclei.

Figure 5 shows[40] the calculated CP and TORQUE curves for $\varepsilon = 0.01$ and $\varepsilon = 1$. The constant spin-lock time for H spins, $t_{const} = t_{SL} + t_{CP}$, in the TORQUE curves is 5.0 ms, and the values of β_F are normalized at $t_{CP} = t_{const}$ in order to compare the shapes of the curves. T_{HF} was kept constant at 0.5 ms, and the relaxation parameters for the various curves used were: (A) $T^H_{1\rho} = 2.5$ ms, $T^F_{1\rho} = 100$ ms, (B) $T^H_{1\rho} = 2.5$ ms, $T^F_{1\rho} = 2.5$ ms, (C) $T^H_{1\rho} = 5.0$ ms, $T^F_{1\rho} = 5.0$ ms, (D) $T^H_{1\rho} = 100$ ms, $T^F_{1\rho} = 2.5$ ms. The CP curves for $\varepsilon = 0.01$ (Figure 5a) correspond to a typical case of ^{1}H → ^{13}C CP or to ^{1}H → ^{19}F CP for materials that are chemically dilute in fluorines but have abundant protons. In this case, it is well known that the decaying slope of the CP curves in a logarithmic scale is principally determined by $-1/T^H_{1\rho}$ in the region where $t_{CP} \gg T_{HF}$, and the influence of $1/T^F_{1\rho}$ on the slope is negligible. This indicates that different $T^H_{1\rho}$ s can be potentially discriminated from the decaying slope of CP curves when ε is much smaller than 1. When the number of fluorine atoms is much smaller than that of ^{1}H in organic molecules, there is no effective direct relaxation path from ^{19}F to the lattice under spin-locked conditions. As a result, the heat capacity of the ^{19}F spin bath is negligibly small, and $T^F_{1\rho}$ is generally much longer than $T^H_{1\rho}$.

On the other hand, the CP curves for $\varepsilon = 1$ (Figure 5b) correspond to a more typical case of ^{1}H → ^{19}F CP with both hydrogen and fluorine in high concentration, because ^{19}F has 100% natural abundance. For example, the N_F/N_H of one of the most popular fluoropolymers, poly(vinylidenefluoride), is 1. These curves show significantly different behavior from those in Figure 5(a). In particular, no difference was observed in the curves of A, C, and D in spite of the large differences in their values of $T^H_{1\rho}$ and $T^F_{1\rho}$. This can be explained by the fact that the decaying slope is principally determined

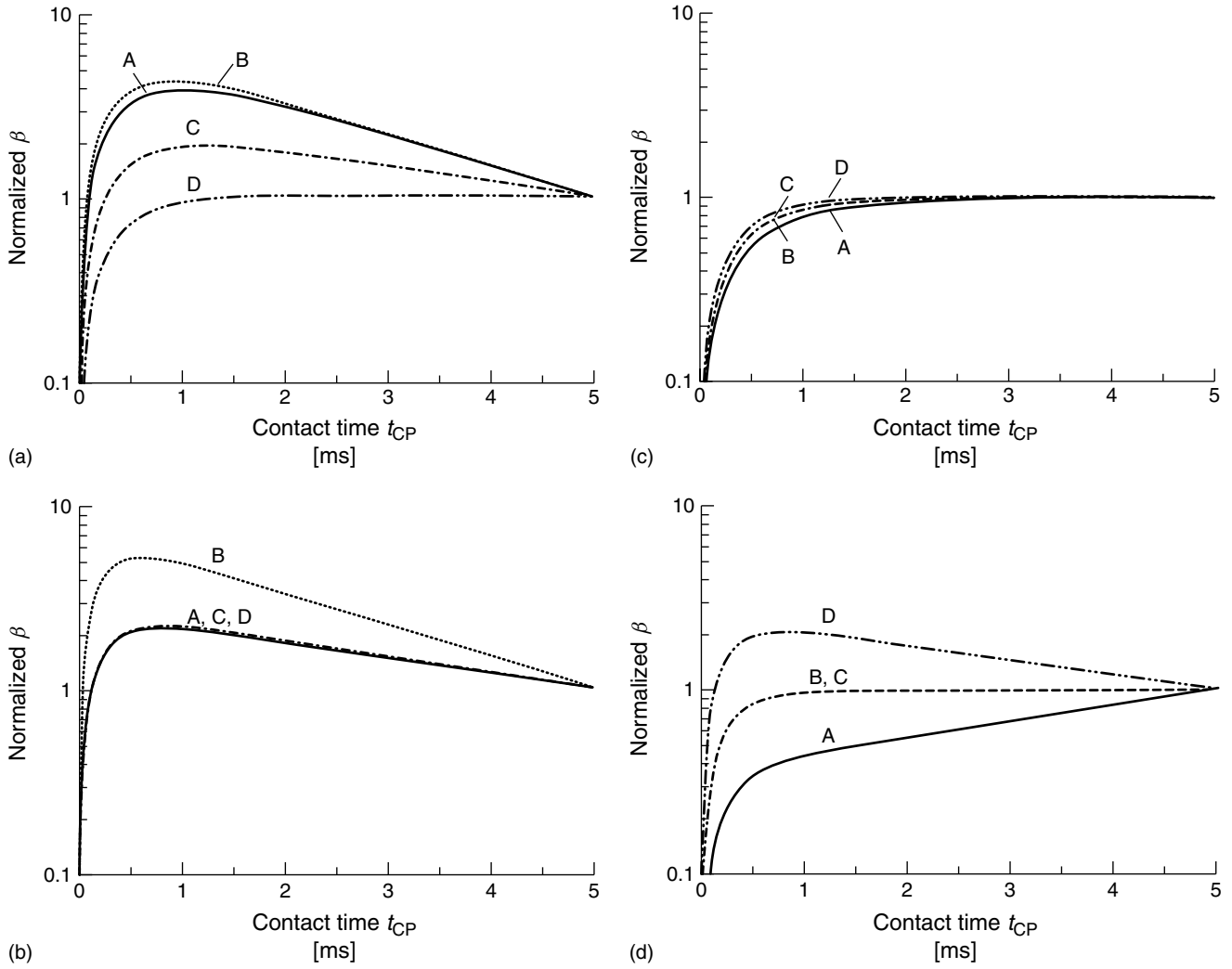

Figure 5 Evolution of the inverse spin temperature (β) for the F bath in the standard H → F CP experiment for (a) $\varepsilon = 0.01$ and (b) $\varepsilon = 1$ and in the H → F TORQUE experiment for (c) $\varepsilon = 0.01$ and (d) $\varepsilon = 1$. These curves were calculated according to equations (5) and (9) as a function of the contact time, t_{CP}, where t_{const} was chosen as 5 ms for TORQUE. All the curves were normalized at $t_{CP} = t_{const} = 5$ ms. T_{HF} was kept constant at 0.5 ms, and the relaxation parameters used, ($T_{1\rho}^{H}$, $T_{1\rho}^{F}$) were (A) (2.5, 100,), B (2.5, 2.5), C (5.0, 5.0) and (D) (100, 2.5), respectively, where the unit is ms. (Reproduced with permission from Ref.[40])

by $(1/T_{1\rho}^{H} + 1/T_{1\rho}^{F})/2$, not by $1/T_{1\rho}^{H}$, when $\varepsilon = 1$ and $1/T_{1\rho}^{F}$ is not negligibly small. The curves A, C, and D actually involve the same value of $(1/T_{1\rho}^{H} + 1/T_{1\rho}^{F})/2$. Consequently, a term involving $1/T_{1\rho}^{F}$ has to be explicitly incorporated into the analysis of CP dynamics between abundant nuclei. The high natural abundance of ^{19}F often makes $T_{1\rho}^{F}$ of the same order as $T_{1\rho}^{H}$. In addition, the heat capacity of the ^{19}F spin bath can be comparable to that of the ^{1}H spin bath when ε is close to 1. Figure 5(b) clearly indicates that CP curves can not discriminate between the three cases of $T_{1\rho}^{H} \ll T_{1\rho}^{F}$, $T_{1\rho}^{H} = T_{1\rho}^{F}$, and $T_{1\rho}^{H} \gg T_{1\rho}^{F}$. This is one of the major reasons that the conventional method can not be applied to analysis of ^{1}H → ^{19}F CP dynamics.

Furthermore, equation (5) can be approximated by the following

$$\left[\frac{\beta_F(t)}{\beta_{H0}}\right]_{CP} = A\left[-\exp\left(-\frac{t_{CP}}{T_{HF}^{*}}\right) + \exp\left(-\frac{t_{CP}}{T_{1\rho}^{*}}\right)\right] \qquad (10)$$

where A is a constant, and T_{HF}^{*} and $T_{1\rho}^{*}$ are effective time constants for the increase and decay of β_F. This indicates that any kind of CP curve for a homogeneous system can be well described by these two constants using the conventional expression. It is well-known that T_{HF}^{*} and $T_{1\rho}^{*}$ are analogous to T_{HF} and $T_{1\rho}^{H}$, respectively, when the following conditions are fulfilled: (1) F is a rare spin, (2) T_{HF} is considerably shorter than $T_{1\rho}^{H}$, and (3) $T_{1\rho}^{F}$ is considerably longer than $T_{1\rho}^{H}$. We will refer to this extreme situation ($\varepsilon \ll 1$ and $T_{HF} \ll T_{1\rho}^{H} \ll T_{1\rho}^{F}$) as the ideal CP condition. However, when ε is not negligibly small and $T_{1\rho}^{F}$ is comparable to $T_{1\rho}^{H}$ (as is frequently true for ^{1}H → ^{19}F CP), no simple relationship is expected between the effective parameters (T_{HF}^{*}, $T_{1\rho}^{*}$) and the true parameters for CP dynamics, T_{HF}, $T_{1\rho}^{H}$, and $T_{1\rho}^{F}$.

Figure 5(c) shows the TORQUE curves calculated for $\varepsilon = 0.01$. The decay of β_F is effectively suppressed in all the cases, indicating that it is mainly caused by $T_{1\rho}^{H}$. The shape of the curves is insensitive to the magnitude of $T_{1\rho}^{F}$. On the other

hand, the TORQUE curves calculated for $\varepsilon = 1$ (Figure 5d) show significantly different behavior from those in Figure 5(c). The decay of β_F can be suppressed only in the cases when $T_{1\rho}^H = T_{1\rho}^F$ (B and C). Otherwise, the slope at $t_{CP} = t_{const}$ is positive for $T_{1\rho}^H \ll T_{1\rho}^F$ (A) and negative for $T_{1\rho}^H \gg T_{1\rho}^F$ (D). This relationship can be mathematically verified.[40] Although the TORQUE sequence does not quench the relaxation process with $T_{1\rho}^H$ when ε is not negligibly small, the sign of the slope should be generally helpful in analyzing CP dynamics between abundant nuclei.

The contact-time dependence of β_H can also be obtained by solving equation (1) under the same initial conditions, giving:

$$\left[\frac{\beta_H(t)}{\beta_{H0}}\right]_{CP} = \frac{1}{a_+ - a_-}\left[-\left(1 + \frac{T_{HF}}{T_{1\rho}^F} - a_+\right)\exp\left(-\frac{a_+}{T_{HF}}t_{CP}\right) + \left(1 + \frac{T_{HF}}{T_{1\rho}^F} - a_-\right)\exp\left(-\frac{a_-}{T_{HF}}t_{CP}\right)\right] \quad (11)$$

This corresponds to the t_{CP} dependence of the residual H magnetization during the H → F CP experiment (which we will refer to as a CP-drain curve).[39] Equation (11) indicates that the residual proton magnetization decays with the same time constants of $-\frac{a_+}{T_{HF}}$ and $-\frac{a_-}{T_{HF}}$ as for the increase in F magnetization expressed by equation (5). The first of these time constants relates to the decrease in H magnetization caused by the polarization transfer to F spins, and the second time constant expresses the decrease caused by the relaxation to the lattice. Accordingly, at the ideal CP condition, the rates of the former and the latter processes are equal to $1/T_{HF}$ and $1/T_{1\rho}^H$.

When T_{HF} is much smaller than $T_{1\rho}^H$ and $T_{1\rho}^F$, the coefficient of the second term in equation (11) is expressed as

$$\frac{1}{a_+ - a_-}\left(1 + \frac{T_{HF}}{T_{1\rho}^F} - a_-\right) = \frac{1}{1+\varepsilon} \quad (12)$$

This indicates that, when the spin-lattice relaxation is very slow, the proportion of the residual magnetization in the H spin bath to the transferred magnetization to the F spin bath after CP is $1/(1+\varepsilon)$. In particular, this term becomes unity at the ideal CP condition.

Equation (11) can also be expressed in terms of effective values in the same way as equation (10). The corresponding equation for fitting CP-drain curves is

$$\left[\frac{\beta_H(t)}{\beta_{H0}}\right]_{CP} = (1 - B)\cdot\exp\left(-\frac{t_{CP}}{T_{HF}^*}\right) + B\cdot\exp\left(-\frac{t_{CP}}{T_{1\rho}^*}\right) \quad (13)$$

It should be noted that the magnitude of the H magnetization can be normalized at $t_{CP} = 0$, which is a distinguishing feature of CP-drain curves. One may deduce additional information from the intensity of CP-drain curves, while only the shape of curves (slopes) can be examined for CP-curves. At the ideal CP condition, the decay of H magnetization is principally characterized by $-1/T_{1\rho}^H$ because $B = 1/(1+\varepsilon)$ is unity and $T_{1\rho}^* = T_{1\rho}^H$. When B takes a value between 0 and 1, this value is related to the proportion of the H magnetization that does not transfer to the F spin bath during H → F CP. As described above, when T_{HF} is much smaller than $T_{1\rho}^H$ and $T_{1\rho}^F$, B can be determined as the intercept of the slower decaying part of the CP-drain curve, which represents the relaxation to the lattice (time constant $= -1/T_{1\rho}^*$), to $t_{CP} = 0$, and this value should be equal to $1/(1+\varepsilon)$.

Furthermore, the comparison between equations (5) and (10) enables one to examine the relationship between T_{HF}^*, T_{HF}, $T_{1\rho}^*$ and $T_{1\rho}^H$ by introducing two parameters, f_1 and f_2.

$$T_{HF}^* = \frac{T_{HF}}{a_+} = \frac{T_{HF}}{a_0 + \sqrt{a_0^2 - b}} = f_1 \cdot T_{HF} \quad (14)$$

$$T_{1\rho}^* = \frac{T_{HF}}{a_-} = \frac{1}{a_0 - \sqrt{a_0^2 - b}}\frac{T_{HF}}{T_{1\rho}^H}\cdot T_{1\rho}^H = f_2 \cdot T_{1\rho}^H \quad (15)$$

The values of f_1 and f_2 can be calculated as functions of three parameters, namely ε, $T_{HF}/T_{1\rho}^H$ and $T_{HF}/T_{1\rho}^F$. At the ideal CP

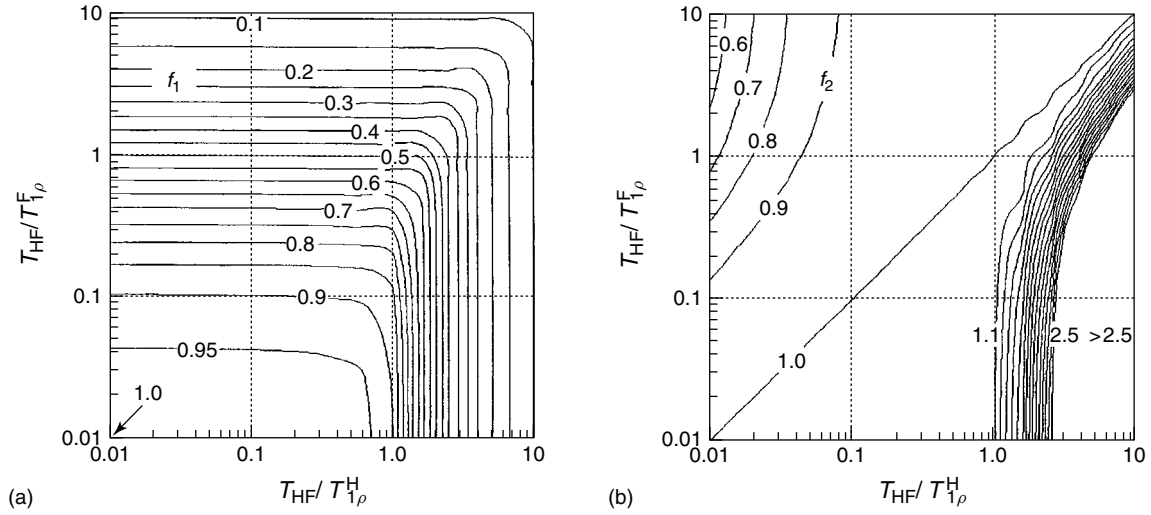

Figure 6 Contour maps of the two parameters f_1 (a) and f_2 (b) that were calculated according to equation (14) and equation (15) for $\varepsilon = 0.01$. These two factors are expressed as functions of $T_{HF}/T_{1\rho}^H$ and $T_{HF}/T_{1\rho}^F$. The limiting value of f_1 at $T_{HF}/T_{1\rho}^H \to 0$ and $T_{HF}/T_{1\rho}^F \to 0$ is 1.0. (Reproduced with permission from Ref.[39])

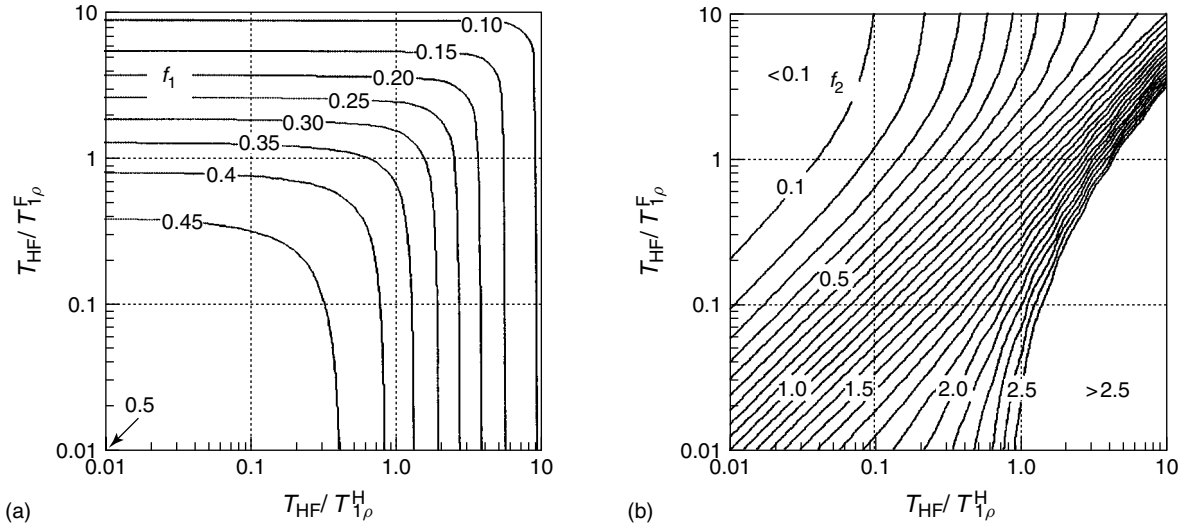

Figure 7 Contour maps of the two parameters f_1 (a) and f_2 (b) calculated for $\varepsilon = 1$. The limiting value of f_1 at $T_{HF}/T_{1\rho}^{H} \to 0$ and $T_{HF}/T_{1\rho}^{F} \to 0 = 0.5$. (Reproduced with permission from Ref.[39])

condition, f_1 and f_2 are unity (see below). Hence, f_1 and f_2 indicate the degree of deviation of the CP dynamics concerned from the ideal CP condition.

Figures 6(a) and 6(b) show the contour maps of f_1 and f_2 calculated using equations (6)–(8) when $\varepsilon = 0.01$, corresponding to the case of chemically dilute fluorines (or to the standard $^1H \to {}^{13}C$ situation). These two factors are expressed as functions of $T_{HF}/T_{1\rho}^{H}$ and $T_{HF}/T_{1\rho}^{F}$. Figure 6(a) indicates that, when $T_{HF}/T_{1\rho}^{H}$ and $T_{HF}/T_{1\rho}^{F}$ are smaller than 0.1, $T_{1\rho}^{*}$ and T_{HF}^{*} are analogous to $T_{1\rho}^{H}$ and T_{HF}, respectively, within an error of 10%. This condition is commonly fulfilled in semi-crystalline and amorphous polymers at temperatures lower than glass transition temperatures. Moreover, $T_{1\rho}^{*}$ has a similar value to $T_{1\rho}^{H}$ in a wide region of the map. These results support the use of the conventional method for the analysis of CP dynamics as long as the conditions described above are fulfilled, so that $T_{1\rho}^{*}$ and T_{HF}^{*} can be taken as $T_{1\rho}^{H}$ and T_{HF}, respectively. On the other hand, Figures 7(a) and 7(b) show the contour maps of f_1 and f_2 calculated when $\varepsilon = 1$, corresponding to many $^1H \to {}^{19}F$ CP situations.

These figures exhibit distinctly different features from those in Figure 6. Even when T_{HF} is one hundredth of $T_{1\rho}^{H}$ and $T_{1\rho}^{F}$, the effective T_{HF}^{*} is only half of T_{HF}. This indicates that the effective ('observed') T_{HF}^{*} is much shorter than the true value of T_{HF} when ε is not negligibly small. By using equation (14), it can be shown that T_{HF}^{*} is equal to $T_{HF}/(1+\varepsilon)$, when T_{HF} is much shorter than $T_{1\rho}^{H}$ and $T_{1\rho}^{F}$. This corresponds to the fact that the rates of the initial increase in the CP-curve and the fast decrease in the CP-drain curve are faster than the respective values of T_{HF}, as seen in Figure 6(b). In addition, f_2 is very sensitive to the variation in $T_{HF}/T_{1\rho}^{H}$ and $T_{HF}/T_{1\rho}^{F}$. This indicates that the $T_{1\rho}^{*}$ value determined from the slope of the experimental decay in the CP curve might not be similar to $T_{1\rho}^{H}$. This result can be explained by the decaying slope of the CP curve being principally determined by $(1/T_{1\rho}^{H} + 1/T_{1\rho}^{F})/2$, not by $1/T_{1\rho}^{H}$, when $\varepsilon = 1$, as described above. This corresponds to the decaying slopes of the CP and CP-drain curves being considerably different from the relevant vales of $T_{1\rho}^{H}$.

The approach described above can be generalized for any number of spin baths.[42] Typically, at modest MAS rates, a single proton spin bath but several fluorine spin baths will exist. This situation occurs when the proton spectrum is homogeneous whereas the relatively large chemical shift differences for ^{19}F ensure that separate signals are observed when proton-decoupling is employed. Under $^1H \to {}^{19}F$ CP conditions, spin exchange between the various ^{19}F spin baths can occur at varying rates (this will include a r.f.-driven CP-like component) (see Figure 8).

Simulations of multiple abundant spin-bath CP are based on a simple extension of the problem of two spin baths. Spins in separate baths, with inverse spin temperatures β_i, β_j etc., may be in contact with each other and with the lattice as seen in Figure 8. Invoking the constraints required by the conservation of energy in the rotation frame and the long-term equilibrium distribution of spin temperatures, the following differential equations can be derived, which are analogous to those in equation (1).

$$\begin{aligned}
\frac{d}{dt}\beta_A &= \frac{1}{T_{AB}}[\beta_B - \beta_A] + \frac{1}{T_{AC}}[\beta_C - \beta_A] + \cdots + \frac{1}{T_{AN}}[\beta_N - \beta_A] - \frac{1}{T_{1\rho}^{A}}\beta_A \\
\frac{d}{dt}\beta_B &= \frac{\varepsilon_{AB}}{T_{AB}}[\beta_A - \beta_B] + \frac{1}{T_{BC}}[\beta_C - \beta_B] + \cdots + \frac{1}{T_{2N}}[\beta_N - \beta_B] - \frac{1}{T_{1\rho}^{B}}\beta_B \\
\frac{d}{dt}\beta_C &= \frac{\varepsilon_{AC}}{T_{AC}}[\beta_A - \beta_C] + \frac{\varepsilon_{BC}}{T_{BC}}[\beta_B - \beta_C] + \cdots + \frac{1}{T_{2N}}[\beta_N - \beta_C] - \frac{1}{T_{1\rho}^{C}}\beta_C \\
&\vdots \qquad\qquad \vdots \qquad\qquad \vdots \qquad\qquad \vdots \qquad\qquad \vdots \\
\frac{d}{dt}\beta_N &= \frac{\varepsilon_{AN}}{T_{AN}}[\beta_A - \beta_N] + \frac{\varepsilon_{BN}}{T_{BN}}[\beta_B - \beta_N] + \cdots + \frac{\varepsilon_{N-1N}}{T_{N-1N}}[\beta_{N-1} - \beta_N] - \frac{1}{T_{1\rho}^{N}}\beta_N
\end{aligned} \tag{16}$$

In matrix form equation (16) is expressed as $\frac{d}{dt}\mathbf{B} = \mathbf{R} \cdot \mathbf{B}$, where $\mathbf{B} = [\beta_A, \beta_B, \beta_{C,\cdots}\beta_N]^T$. This system of equations can be solved as $\mathbf{B}(t) = \exp(\mathbf{M}t) \cdot \mathbf{B}(0)$ where $\mathbf{M}$ is the matrix shown in equation (17).

$$\begin{bmatrix} -\frac{1}{T_{AB}} - \frac{1}{T_{AC}} - \cdots - \frac{1}{T_{AN}} - \frac{1}{T_{1\rho}^{A}} & \frac{1}{T_{AB}} & \frac{1}{T_{AC}} & \cdots & \frac{1}{T_{AN}} \\ \frac{\varepsilon_{AB}}{T_{AB}} & -\frac{\varepsilon_{AB}}{T_{AB}} - \frac{1}{T_{BC}} - \cdots - \frac{1}{T_{BN}} - \frac{1}{T_{1\rho}^{B}} & \frac{1}{T_{BC}} & \cdots & \frac{1}{T_{BN}} \\ \frac{\varepsilon_{AC}}{T_{AC}} & \frac{\varepsilon_{BC}}{T_{BC}} & -\frac{\varepsilon_{AC}}{T_{AC}} - \frac{\varepsilon_{BC}}{T_{BC}} - \cdots - \frac{1}{T_{CN}} - \frac{1}{T_{1\rho}^{C}} & \cdots & \frac{1}{T_{CN}} \\ \vdots & \vdots & \vdots & \ddots & \vdots \\ \frac{\varepsilon_{AN}}{T_{AN}} & \frac{\varepsilon_{BN}}{T_{BN}} & \frac{\varepsilon_{CN}}{T_{CN}} & \cdots & -\frac{\varepsilon_{AN}}{T_{AN}} - \frac{\varepsilon_{BN}}{T_{BN}} - \cdots - \frac{\varepsilon_{N-1N}}{T_{N-1N}} - \frac{1}{T_{1\rho}^{N}} \end{bmatrix} \tag{17}$$

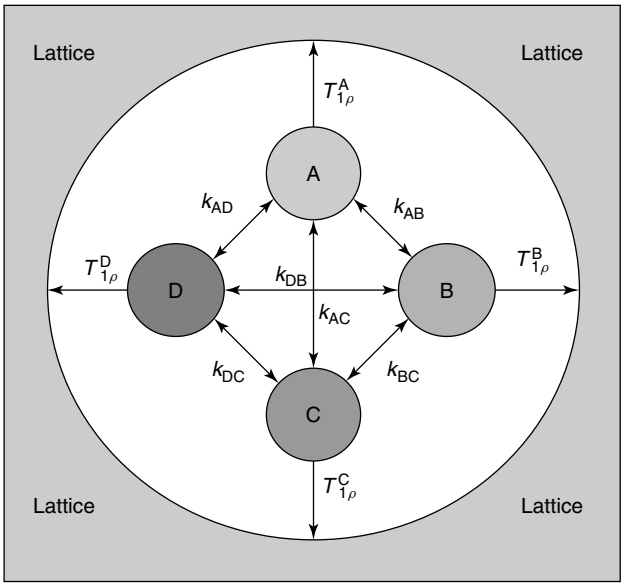

Figure 8 Diagrammatic view of cross-polarization dynamics for a system of four spin baths where one of them, A say, is initially produced in a non-equilibrium state by a 90° pulse. Each spin bath is characterized by an inverse spin temperature, β, and a relative population, ε

Exp(**M**) can be evaluated as $\boldsymbol{\Lambda}^{-1} \cdot \exp(\mathbf{D}) \cdot \boldsymbol{\Lambda}$ where **D** is the matrix of eigenvalues and $\boldsymbol{\Lambda}$ is the matrix of eigenvectors.

A computer program has been written,[42] using equation (17), to iteratively fit CP curves to yield values of characteristic inter-bath spin-exchange times (T_{HF} and T_{FF}), using separately measured values of $T_{1\rho}^{H}$ and $T_{1\rho}^{F}$ as part of the input.

4 FLUOROPOLYMERS

There have been four comprehensive reviews[1,2,43,44] in the last decade relating to the high-resolution ^{19}F NMR of fluoropolymers containing hydrogen. In 1987, a pioneering work on high-resolution ^{19}F MAS NMR at spin rates between 18 and 22 kHz was reported by Dec et al.[13] for copolymers of vinylidenefluoride (CF_2CH_2, VDF) and hexafluoropropylene (CF_3CFCF_2, HFP) and of VDF and chlorotrifluoroethylene (CF_3CFCl), and for terpolymers of VDF, HFP, and tetrafluoroethylene (CF_2CF_2, TFE). Structural assignments of chemical shifts in terms of pentad sequences were made on the basis of solution-state NMR. Recently, Isbester et al.[45] recorded ^{19}F NMR spectra for the same kinds of polymers by simultaneously using MAS rates up to 25 kHz and heating to 250 °C. Very high resolution was achieved at the higher temperatures,[46] and the peaks were assigned by comparison to results from solution-state NMR studies. Detailed monomer compositions of six polymers were quantitatively determined. The authors reported that equivalent resolution was observed for a copolymer if a spectrum acquired at a spin rate of 19 kHz is compared to the corresponding spectrum acquired at 4 kHz and a 50 °C higher temperature.

Harris and coworkers[22,24–27,30,39,40,47,49] have conducted a number of high-resolution ^{19}F NMR studies utilizing MAS, cross polarization (CP), and high-power proton/fluorine decoupling. In particular, several efforts have been devoted to poly(vinylidene fluoride) (PVDF) because of its interesting polymorphism and dielectric properties. The results from ^{19}F–pulsed, ^{19}F wideline, ^{19}F MAS and ^{1}H → ^{19}F CP/MAS NMR of PVDF, all with high-power proton decoupling, have been reviewed in detail.[2] Holstein et al.[24] have reported that, with ^{1}H decoupling, PVDF powder obtained from the melt shows, at ambient probe temperature, a major signal (peak I in Figure 9(c)), together with shoulders (on both high-frequency and low-frequency sides, II and III) and a weak doublet at lower frequency (peaks IV and V). The weak doublets were assigned to chain imperfections of *head-to-head* and *tail-to-tail* sequences, and the shoulders arise from crystalline regions.

The authors[24] showed that discrimination in favor of the crystalline regions can be obtained by spin-locking the protons prior to CP contact because $T_{1\rho}^{H}$ is substantially shorter for amorphous chains. On the other hand, discrimination in favor of the amorphous region was achieved by the dipolar dephasing pulse sequence because the hetero-nuclear dipolar interaction is substantially stronger for crystalline chains. Figure 9(b) shows a spectrum of the amorphous (mobile)

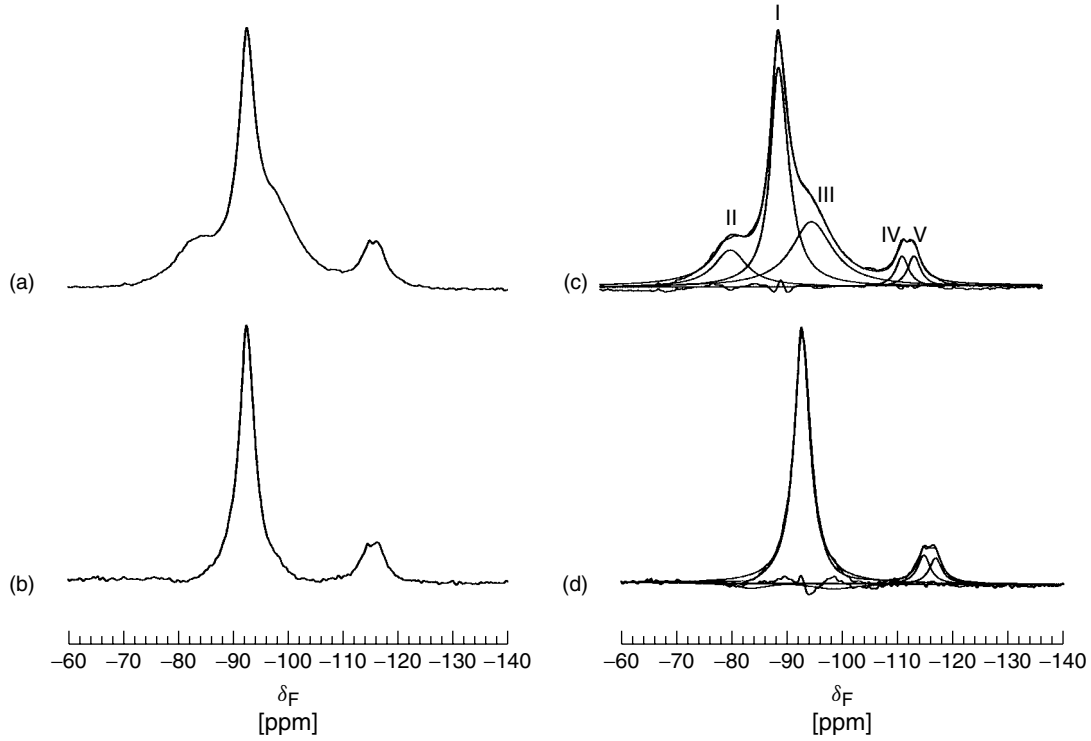

Figure 9 188.29 MHz ^{19}F spectra of solid PVDF powder using (a) $^{1}H \rightarrow {}^{19}F$ CP and (b) the DIVAM (discrimination induced by variable amplitude minipulses) pulse sequence, both obtained at a spin rate of 13.5 kHz with high-power ^{1}H decoupling. The DIVAM CP pulse sequence selectively observes the amorphous region. The spectra **c** and **d** show deconvolutions of **a** and **b** respectively, obtained using Lorentzian functions. For a discussion of the peaks I to V, see the text. (Reproduced with permission from Ref.[49])

domains obtained with an alternative pulse sequence.[49] This indicates that the imperfections are largely or wholly in the amorphous regions. Scheler et al.[22] have applied the two-dimensional (^{1}H and ^{19}F) wideline separation (WISE) sequence[21] to PVDF, both with and without ^{19}F–decoupling during the ^{1}H evolution time. The resulting spectra exemplify the mobility differences between the amorphous and α-crystalline chains. The signals from crystalline and amorphous regions were clearly distinguished in the proton lineshapes and the second moments of the lines. The selection of subspectra from the amorphous and crystalline parts of the polymer by dipolar and $T_{1\rho}$ filters, respectively, strongly supports the assignments.

There are two major crystalline forms, denoted α and β, in PVDF. The chains of the α-form have the $tg^{+}tg^{-}$ conformation, whereas those in the β-form have the all-*trans* conformation. Holstein et al.[25] have studied samples with partial conversion of the α-form to the β-form (obtained by uniaxial or biaxial drawing) and have shown that the β-form gives a single signal at $\delta_F = -98$ ppm whereas the α-form give two signals at $\delta_F = -82$ ppm (peak II) and -98 ppm (peak III), as described above. The immobile chains in the crystalline regions required the application of proton high-power decoupling to completely remove proton–fluorine interactions. The origin of the chemical shifts can be well understood in terms of the γ-gauche effect. Scheler[15] has shown that magic-angle spinning at 30 kHz or more adequately averages (H,F) as well as (F,F) dipolar interactions for PVDF giving high-resolution ^{19}F spectra. This removes the requirement for high-power proton decoupling. Scheler[15] also showed that the two-dimensional RFDR technique provides a simple test for the spatial proximity of different types of fluorines and thus enables the domain structure of PVDF to be explored. However, for the RFDR experiment proton decoupling is essential even at the highest spinning speeds because the recoupling pulses also recouple heteronuclear coupling.

Su and Tzou[48] have also examined the polymorphism of PVDF using fast MAS with spin speeds up to 35 kHz without ^{1}H decoupling. They were thus able to estimate the proportions of the crystalline region, amorphous region, and defect segments as 41%, 54%, and 5% respectively. The authors also analyzed spinning sideband manifolds in PVDF ^{19}F spectra obtained at very high magnetic fields (752.8 MHz frequency) to yield shielding tensor principal components for the different signals, though they do not seem to have taken into account any effects from (H,F) or (F,F) dipolar interactions on sideband intensities. They show that the two peaks assigned to crystalline regions have different shielding tensors, and that their shielding anisotropies are significantly larger than that of the amorphous peak, as commented earlier by Holstein et al.[25] Like Scheler,[15] Su and Tzou[48] used 2D spin-diffusion experiments to indicate proximity between the fluorine sites giving the crystalline-phase signals, and also between the fluorines in the defect structures and those of the amorphous regions. Ando et al.[49] have measured ^{19}F spin-lock, $^{1}H \rightarrow {}^{19}F$ CP, and $^{1}H \rightarrow {}^{19}F$ inversion recovery CP (IRCP) MAS spectra of PVDF to give proton and fluorine relaxation times ($T_{1\rho}^{F}$, $T_{1\rho}^{H}$) and effective parameters (T_{HF}^{*}, $T_{1\rho}^{*}$) relating to $^{1}H \rightarrow {}^{19}F$ CP (Figure 10).

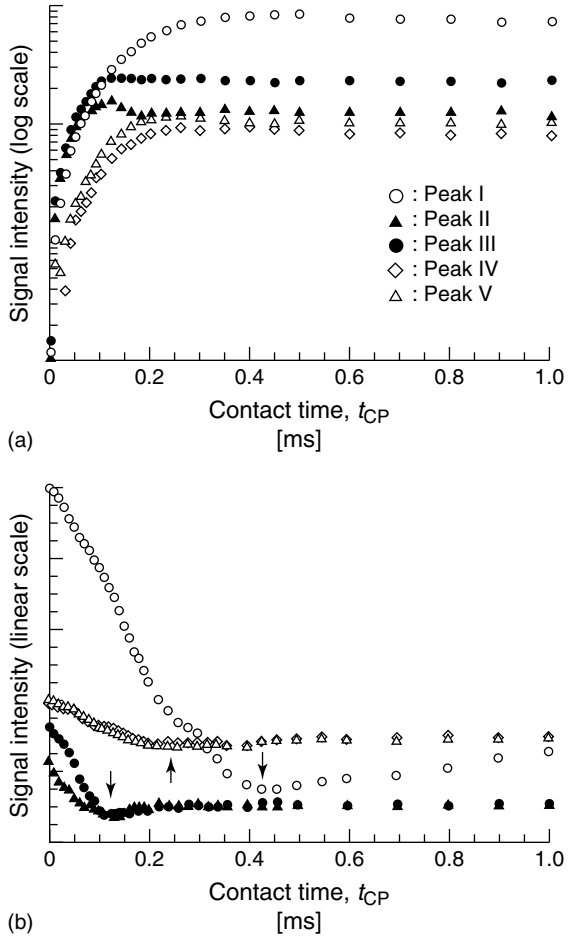

Figure 10 Dependence of the ^{19}F signal intensities for (a) $^{1}H \rightarrow {}^{19}F$ CP and (b) $^{1}H \rightarrow {}^{19}F$ IRCP experiments on PVDF at short contact times with MAS at 13.5 kHz and for $B_o = 4.7$ T. The pre-contact time of the IRCP was 0.2 ms, and the signal intensities of peaks II and III are displaced downwards in (b) to avoid overlap of symbols. The dips originating from the dipolar oscillation behavior are indicated by arrows. Reproduced with permission of Ref.[49]

The values of $T_{1\rho}^{F}$, $T_{1\rho}^{H}$ and $T_{1\rho}^{*}$ for peaks II and III in Figure 9 (crystalline region) are larger than those of peaks I, IV, and V (amorphous region), whereas the values of T_{HF}^{*} for the former pair of peaks are significantly shorter than those of the latter set of peaks. These facts coincide well with the stronger heteronuclear dipolar interactions in the crystalline region of PVDF. Although there is no difference in the spin dynamics between the CP and IRCP experiments, IRCP is superior to the standard CP in observing details of CP processes. The dipolar oscillations in the ^{19}F spectral intensities are clearly observed in the initial stage for IRCP not only for the crystalline peaks, but also for the amorphous peaks (Figure 10b). The first dips observed for peaks II and III are at 0.125 ms, while that for peak I is at 0.425 ms and those for peaks IV and V are around 0.25 ms. The effective average F–H bond distances calculated from these values are 2.2 Å, 3.3 Å, and 2.7 Å, respectively. The longer effective distances in the amorphous peaks are straightforwardly ascribed to molecular motion of the order of several tens of kHz. In addition, the authors[49] measured the $^{19}F \rightarrow {}^{1}H$ CP MAS spectrum of PVDF. The spinning sidebands originate from the residual dipolar interactions that are not averaged out by MAS at a spin rate of 13.5 kHz. Although the main peak and spinning sidebands can be fitted by single Lorentzian functions, the half-height width (hhw) of the former (900 Hz) is significantly smaller than those of the latter (ca. 3000 Hz). This suggests that the contribution of the amorphous signal is mostly limited to the main peak, while that of the crystalline signal is distributed to both the centreband and sidebands. The $^{19}F \rightarrow {}^{1}H$ CP dynamics (especially the effective parameter, T_{FH}^{*}) and the dipolar oscillation behavior, which is only observed for the sidebands, support this view. This phenomenon coincides well with the fact[27] that the spinning sidebands in a ^{1}H-decoupled ^{19}F MAS spectrum at a spin rate of 12 kHz contribute substantially to the spectra of the crystalline region.

Monti et al.[47] have investigated ^{19}F MAS and $^{1}H \rightarrow {}^{19}F$ CP/MAS NMR spectra of Viton-type fluoroelastomers (Figure 11), which are copolymers of VDF and HFP, and terpolymers containing TFE units also.

The $^{1}H \rightarrow {}^{19}F$ CP and TORQUE curves were well fitted by modified conventional equations, and different effective parameters were obtained for five separate peaks, which gave some insight into the CP dynamics between protons and fluorines, although the high abundance of fluorine atoms and efficient $T_{1\rho}^{F}$ process were not explicitly considered. Ando et al.[40] also measured $^{1}H \rightarrow {}^{19}F$ CP/MAS spectra of a Viton-type fluoroelastomer and reexamined the CP dynamics between ^{1}H and ^{19}F using the exact solutions of the equations for the spin thermodynamics. Simultaneous fitting of the evolution of magnetization in the standard CP and TORQUE experiments (Figure 12) gave unique sets of the parameters T_{HF}, $T_{1\rho}^{H}$, and $T_{1\rho}^{F}$ for the five separate peaks in the ^{19}F spectra.

The values of $T_{1\rho}^{H}$ and $T_{1\rho}^{F}$ are consistent with those independently measured by spin-locking experiments. The true values of T_{HF} are significantly larger (by a factor of ca. 4) than the values of T_{HF}^{*} derived from a simple two-parameter fit of the CP behavior with variable contact time.

Ando et al.[39] have also measured (Figure 13) ^{19}F MAS, $^{1}H \rightarrow {}^{19}F$ CP, and $^{1}H \rightarrow {}^{19}F$ CP-drain MAS spectra for a fluorinated polyimide, 6FDA/ODA. The CP dynamics between ^{1}H and ^{19}F for the polyimide (Figure 13) were analyzed

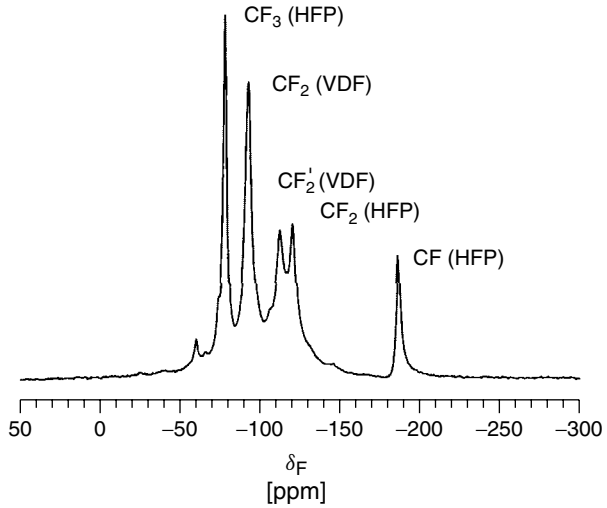

Figure 11 188.29 MHz fluorine-19 MAS spectrum of Viton obtained with proton decoupling, together with the assignments of the peaks

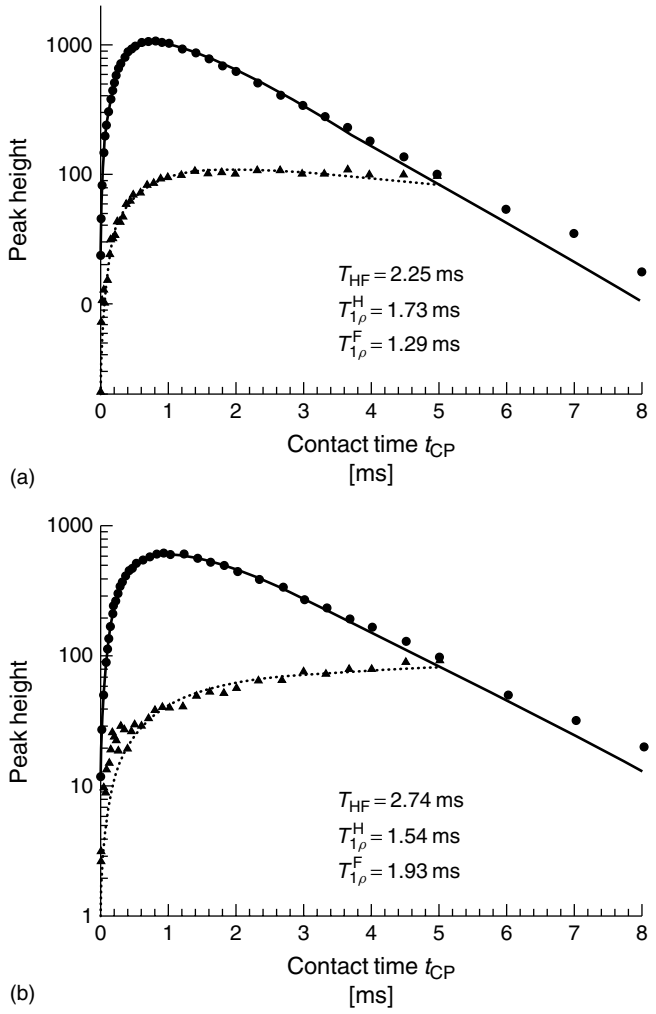

Figure 12 Simultaneous fitting of CP and TORQUE curves for CF_2 of VDF and CF of HFP units. Unique sets of three parameters (T_{HF}, $T_{1\rho}^{H}$, $T_{1\rho}^{F}$) were determined as shown in the figures. Filled circles and triangles represent the signal intensities obtained from the conventional CP and TORQUE experiments, respectively, and solid and dotted lines represent the fitted curves. (Reproduced with permission from Ref.[40])

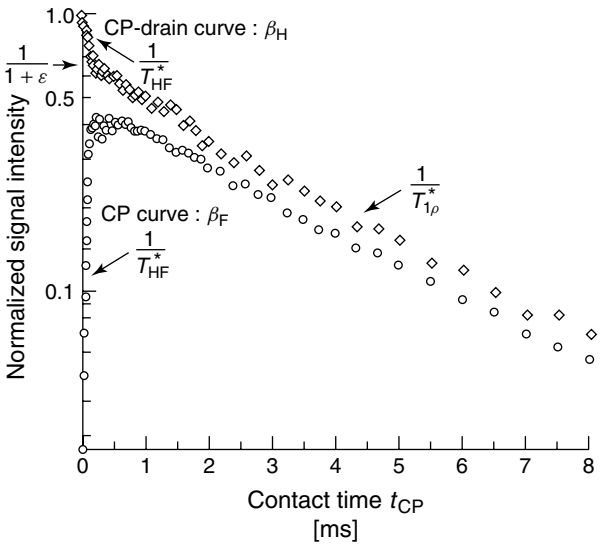

Figure 13 Contact time dependence of the ^1H signal intensity for the $^1H \rightarrow {}^{19}F$ CP (circles) and the $^1H \rightarrow {}^{19}F$ CP-drain (diamonds) experiments at $B_o = 4.7$ T on the fluorinated polyimide. They show the double-exponential behavior, and the value of ε ($=N_F/N_H$) can be calculated from the intercept of the slowly decaying line of the CP-drain curve to $t_{CP} = 0$

on the basis of the spin-thermodynamics theory described in the former section. The constant for polarization transfer (T_{HF}) was determined by the analysis using the effective CP parameters (T_{HF}^*, $T_{1\rho}^*$) together with independently measured values of $T_{1\rho}^{H}$ and $T_{1\rho}^{F}$. The CP-drain experiment, which can measure evolution of residual ^1H magnetization after $^1H \rightarrow {}^{19}F$ CP, was developed, and the value of ε thus obtained (0.49) was close to that determined from the chemical structure ($N_F/N_H = 0.43$) (Figure 13).

Reinsberg et al.[30] have examined ^{19}F MAS, $^1H \rightarrow {}^{19}F$, and $^1H \rightarrow {}^{13}C$ CP/MAS spectra of semi-crystalline poly(trifluoroethylene) (PTrFE). The ineffectiveness of the selection schemes between crystalline and amorphous regions ($T_{1\rho}$–filter and dipolar dephasing) indicates that relaxation parameters differ by less than an order of magnitude. The α-relaxation at ca. 50 °C was proved by a steep decrease of the $^1H \rightarrow {}^{19}F$ CP efficiency for the CF_2 fluorines. The dipolar oscillation frequencies in $^1H \rightarrow {}^{13}C$ CP curves were used to infer the motion of the polymer chain through effective bond distances, and it was concluded that the localized motion of the main chain is considerably hindered at −30 °C.

Ando et al.[26] have investigated $^1H \rightarrow {}^{19}F/{}^{19}F \rightarrow {}^1H$ CP/MAS and ^1H fast MAS spectra of semi-crystalline poly(vinylfluoride) (PVF). Significant differences in $T_{1\rho}^{F}$ and $T_{1\rho}^{H}$ were observed between the immobile and mobile regions, and the effective time constants, T_{HF}^* and $T_{1\rho}^*$ estimated from the $^1H \rightarrow {}^{19}F$ CP curves also clarify the difference in the strengths of dipolar interactions. The inverse $^{19}F \rightarrow {}^1H$ CP-MAS and $^1H \rightarrow {}^{19}F$ CP-drain MAS experiments also gave complementary information to the $^1H \rightarrow {}^{19}F$ CP-MAS spectra, although spinning at 35 kHz is necessary to separate the signals between CHF and CH_2 protons in the ^1H spectra. The dipolar oscillation frequency observed for a crystalline peak in the $^1H \rightarrow {}^{19}F$ CP spectrum correlates well with the H–F distance for a CHF group.

Mabboux and Gleason[50] have studied electron-beam-irradiated vinylidene fluoride/trifluoroethylene (VDF/TrFE) copolymers using high-speed (up to 25 kHz) high-temperature (up to 170 °C) MAS ^{19}F NMR in order to characterize the structure of the polymer. No peaks assigned to crosslinks were resolved, though the crosslinking was implied by linewidth effects. Lau and Gleason[51,52] have reported ^{19}F MAS NMR measurements of films obtained from pulsed plasma-enhanced chemical vapor deposition from hydrofluorocarbon gases, CHF_2CHF_2 and CH_2F_2 at a spin rate of 25 kHz and analyzed their chemical compositions. Various network sequences, namely three CF_3 (CF_3^*C, CF_3^*CF, $CF_3^*CF_2$), five CF_2 ($CF_2CF_2^*CF_2$, $CF_2CF_2^*CF_3$, $CF_2CF_2^*CHF_2$, $CF_2CF_2CF_2^*$, $CF_xCF_2^*CF_x$), and three CF (CF*, CH_2F^*, CF*=C<) segments, were identified in the spectra. Fluorine-19 spin-echo NMR measurements with long delay times (6 ms) were used for selective detection of the mobile region with slower transverse relaxation. In addition, the CF_2 peaks suffered significantly

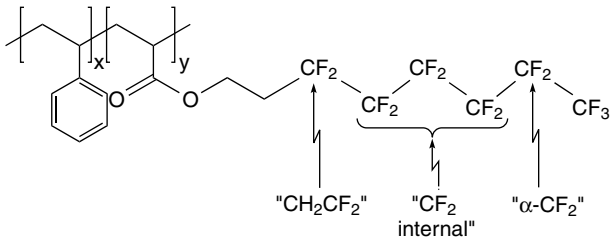

Figure 14 Schematic chemical structure of copoly, which has $x:y = 70:30$. The signals from the three CF_2 groups marked as 'internal' are unresolved, so these fluorines are treated as a single spin-bath

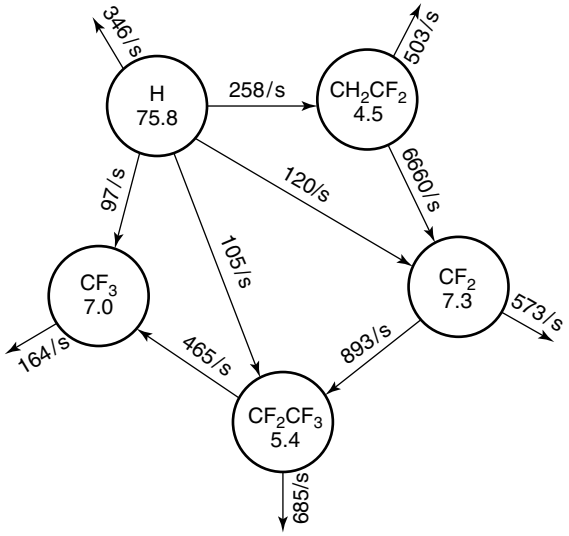

Figure 15 Diagram of the spin baths used for the copoly, with the values for the various rate constants obtained by simultaneously fitting the contact-time curves as shown in Figure 16. The spin-bath populations are also given (in %)

greater intensity loss by spin-echo experiments compared to the CF_3 and CHF peaks, which indicates that the latter groups are relatively more mobile.

The iterative fitting of a multiple spin-bath situation, as described in the previous section, has been applied[42] to the fluoropolymer shown in Figure 14 (which will be referred to as copoly). This system was treated as a problem involving five spin baths, as shown in Figure 15. The corresponding CP curves, Figure 16, were fitted using a program written in MATLAB. The various CP rate parameters, given in Figure 15 were optimized using the Levenberg-Marquardt non-linear least-squares routine.[53] Separately measured $T_{1\rho}$ values were used as constraints. The $^1H \rightarrow {}^{19}F$ CP rates are indicative of the structure of the fluorocarbon sidechain.

5 FLUORINATED ORGANIC COMPOUNDS

In addition to their practical importance, small organic molecules play an essential role as model systems to study NMR effects. Some examples of such use as models will be discussed below. Their major advantage is that they usually exhibit a high degree of crystallinity. On the other hand, the absence of significant motional averaging requires the application of all relevant line-narrowing techniques to obtain high-resolution solid-state spectra.

The large chemical shift range of ^{19}F results in a strong dependence of the Larmor frequency on the chemical environment. This implies the presence of information about both the chemical structure and the spatial arrangement. Therefore, fluorine chemical shifts appear to provide an appropriate tool to study polymorphism. It is also possible to use two-dimensional correlation techniques for the assignment of the signals of the respective forms.

The first applications of $^{19}F-\{^1H\}$ MAS NMR to monofluorinated organic solids were carried out by Hagaman.[7] However, this author reported no ^{19}F high-resolution spectra, but only ^{19}F transverse relaxation times for several different chemical types, including the dependence of T_2 on proton decoupling power. Contemporaneously and independently, Harris and co-workers[8,54] studied three solid fluorinated steroids by $^{19}F-\{^1H\}$ MAS NMR, including a system containing three non-equivalent fluorines. They showed that the technique offered considerable advantages over $^{13}C-\{^1H\}$ NMR for detection and study of polymorphism. The preliminary communication[8] was followed by a full article[10] discussing the methodology of the $^{19}F-\{^1H\}$ experiment, using the fluorinated steroids as examples, and discussing, inter alia, questions of decoupling efficiency, cross-polarization, ^{19}F shielding tensors, spin-lattice relaxation, spin diffusion, dipolar dephasing and rotational resonance. A further article by the same group reported results for a wider range of fluoro-organic systems.[9]

Vierkötter[11] recognized, for the first time, the significant influence (at low or moderate static magnetic fields) of the Bloch-Siegert effect on $^{19}F-\{^1H\}$ spectra of solids (not generally detectable for other solid-state experiments such as $^{13}C-\{^1H\}$). She showed that significant line-broadening of ^{19}F peaks arises from this effect if the sample is not confined to a small volume, because of inhomogeneities in B_1.

Further facets of solid-state $^{19}F-\{^1H\}$ NMR have been illustrated using urea or thiourea inclusion compounds containing fluoro-organic guests.[55–59] Thus, the rate of ring inversion of fluorocyclohexane was studied[55,56,58] by bandshape-fitting, selective polarization inversion, EXSY spectra and $T_{1\rho}$ measurements over a range of temperatures (Figure 17), yielding the thermodynamic parameters for the barrier.

Linear difluoroalkanes in urea inclusion compounds are disordered in the guest arrangements and $^{19}F-\{^1H\}$ NMR proves[56,57] to be a powerful technique to measure average intermolecular (F,F) distances because ideal isolated two-spin systems are involved.[56,57] Static MREV-8 and CPMG experiments yield separate information on dipolar coupling and shielding anisotropy, enabling the simple static pattern to be successfully simulated. The resulting data were used to discuss the distribution of end-group conformations in these systems, taking into account rapid molecular motion about the tunnel axis. MELODRAMA experiments gave[56,59] similar information about dipolar coupling constants for difluoroalkane-urea inclusion compounds.

In the MAS spectrum of 5-fluoro-2-trifluorobenzoic acid (Scheme 1) the signals of the CF and CF_3 fluorines are clearly distinguishable.[35] The existence of two different molecules in the asymmetric unit is shown by the appearance of two sets of lines for each of the CF and CF_3 groups, as depicted in

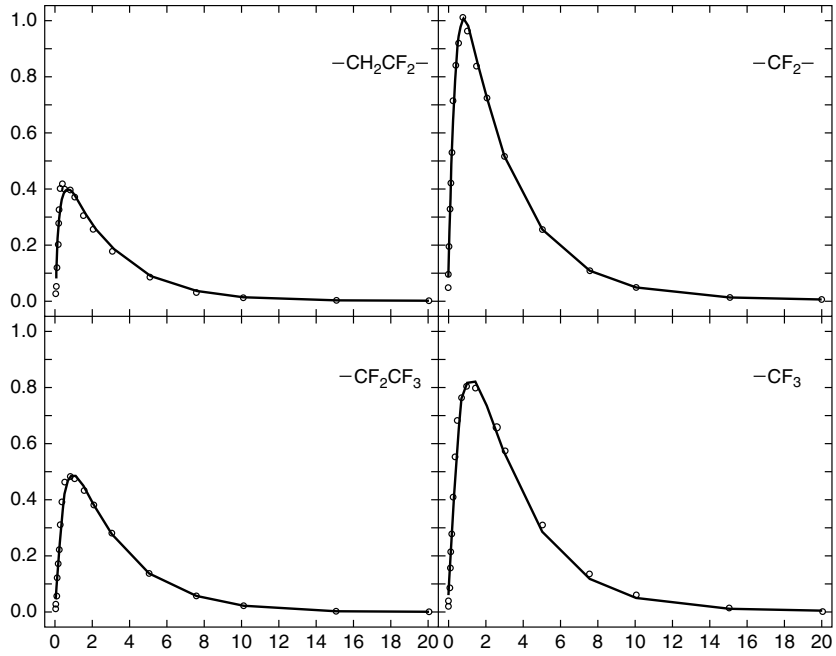

Figure 16 Fitted contact-time $^{1}H \rightarrow {}^{19}F$ CP curves for the four ^{19}F spin-baths of copoly, using the theory discussed in the text. (Reproduced from Ref.[42] by permission of the PCCP Owners Societies)

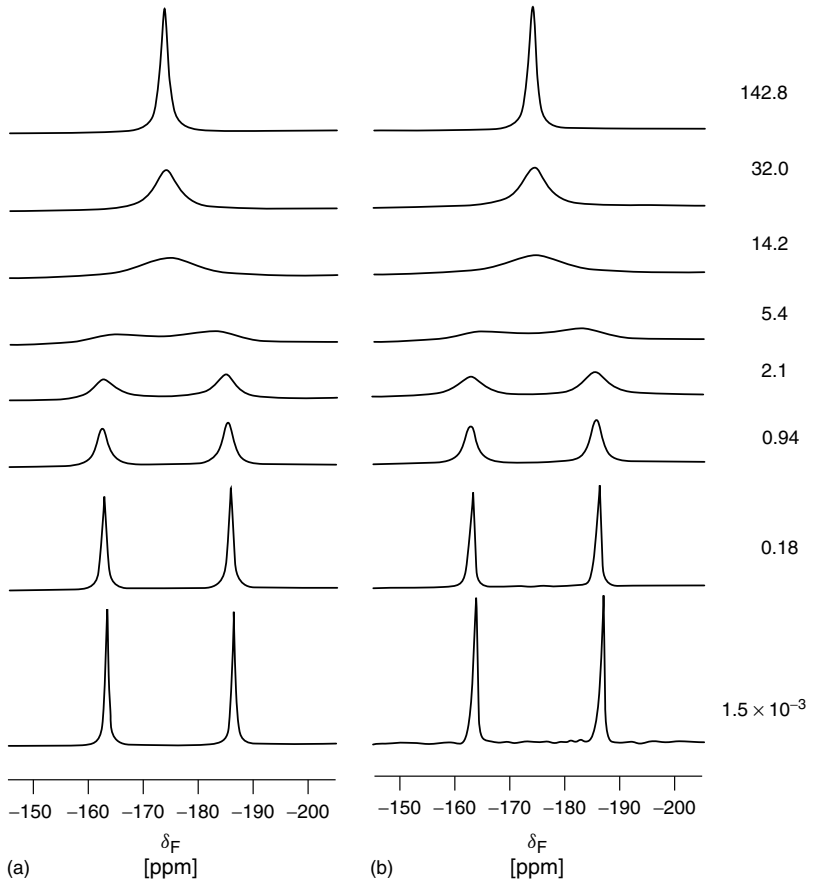

Figure 17 (a) Simulated and (b) experimental 188.29 MHz ^{19}F NMR spectra of fluorocyclohexane in its solid thiourea inclusion compound recorded at (from bottom to top) 177, 217, 237, 247, 258, 268, 278 and 300 K, with the average ring-inversion rate constants given in ms^{-1} down the right-hand side. The rate constants for 177 and 217 K were obtained using the SPI experiment. (Reproduced with permission from Ref.[58])

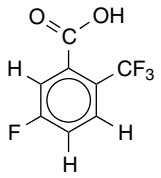

Scheme 1

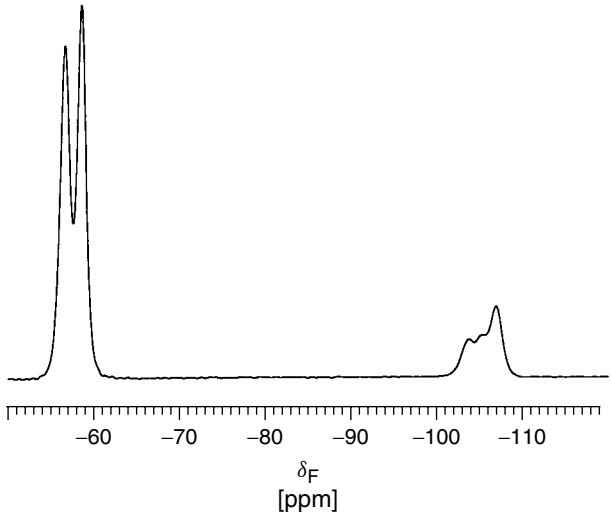

Figure 18 Fluorine-19 MAS NMR spectrum of 5-fluoro-2-(trifluoromethyl)benzoic acid acquired at a Larmor frequency of 282 MHz and a sample spinning frequency of 32 kHz

Figure 18. A possibility to assign the pairs of signals originating from the respective forms is by spin-exchange based on RFDR (radio-frequency driven recoupling).[60] This experiment probes spatial proximity by the distance-dependence of the direct dipolar coupling. Cross-peaks off the diagonal, as seen in Figure 19, are an indication of spin exchange during the mixing time, mediated by the direct dipolar coupling and thus spatial proximity. Normally this will link resonances for the same molecule of the asymmetric unit, though sometimes the intermolecular dipolar interactions may be sufficiently strong

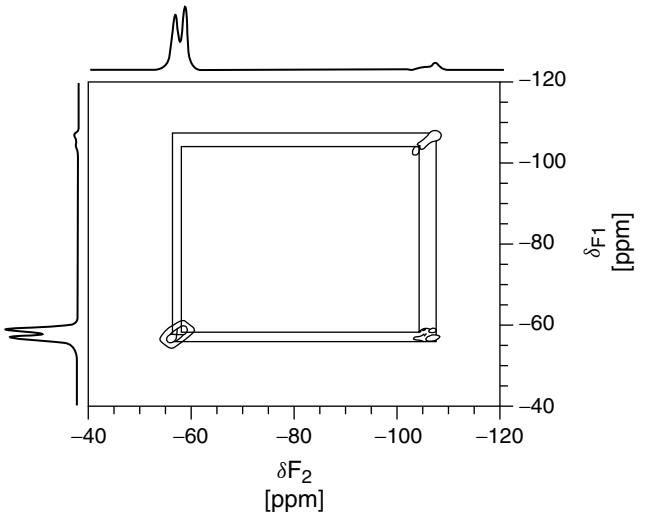

Figure 19 Fluorine-19 spin-exchange experiment under radio-frequency driven recoupling for 5-fluoro-2-(trifluoromethyl)benzoic acid, acquired at a Larmor frequency of 282 MHz with a sample spinning frequency of 32 kHz and a mixing time of 0.5 ms

to confuse matters, as is usual for any experiment exploiting the direct dipolar coupling. In this recoupling experiment proton decoupling during the mixing time is essential, because the recoupling would recouple the heteronuclear dipolar coupling as well, and thus suppress the total signal. The same type of information is available using double-quantum NMR[61] as depicted in Figure 20.[62] In these spectra the chemical shift in the single quantum, directly-detected, dimension is correlated with the double-quantum signal in the indirect dimension, in which the sum of the chemical shifts of the coupled nuclei appears. For double-quantum coherence in a spectrum of spin one-half nuclei, two spins must be coupled. Again, the coupling involved is the distance-dependent direct dipolar effect. The presence of double-quantum coherence is an indication of spatial and spectral proximity. The strength of the dipolar coupling and thus the distance between the coupled nuclei can be determined from a comparison of the spinning sideband pattern in the double-quantum dimension with simulations.

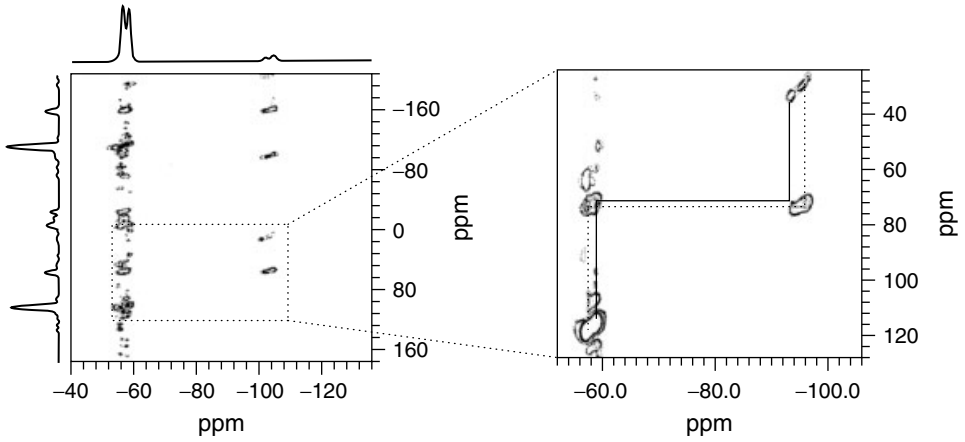

Figure 20 Fluorine-19 double-quantum experiment for 5-fluoro-2-(trifluoromethyl)benzoic acid, acquired at a Larmor frequency of 282 MHz with a sample spinning frequency of 32 kHz using back-to-back pulses with an excitation time of 15 μs. The extra lines in the expansion indicate the link between the CF and CF_3 signals

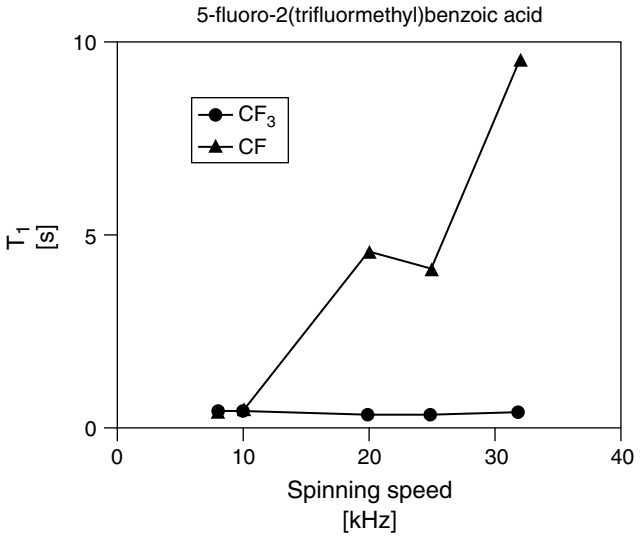

Figure 21 Fluorine-19 longitudinal relaxation times of the CF and CF_3 signals for 5-fluoro-2-(trifluoromethyl)benzoic acid as a function of the sample spinning frequency, obtained at a Larmor frequency of 282 MHz

Miyoshi et al. recently investigated[34] the dependence on MAS rate of T_1 in partially fluorinated derivatives of benzoic acid. In these systems, the fast rotation of a trifluoromethyl group provides an efficient relaxation sink for ^{19}F. At moderate sample spinning rates, there is sufficient overlap of the signals from the trifluoromethyl group and the single fluorine spin on the benzene ring to facilitate spin diffusion and thus fast T_1 relaxation of the isolated fluorine. At higher spinning speeds (Figure 21), there is considerable averaging of both the homonuclear and the heteronuclear dipolar coupling to achieve well-separated lines. This means spin flip-flops are no longer energy-conserving, and therefore spin diffusion is efficiently quenched by MAS. This results in a substantially longer T_1 for the isolated fluorine, which can be as large as 20 s. Although no proton decoupling was applied, it is understood that both homonuclear and heteronuclear coupling influence fluorine spin-diffusion. In most perfluorinated systems (such as fluoropolymers), which have a higher fluorine density, the same mono-exponential T_1 has been observed[63] for all resolved sites, even under high-speed MAS. This fact is attributed to spin-diffusion, which is rapid on the time scale of T_1. The same group of compounds has been used[34] to test and calibrate internuclear distance measurements using Lee–Goldburg cross-polarization between ^1H and ^{19}F. The results nicely correspond to the distances determined in molecular simulations.

Another example for monitoring fluorine spin diffusion is provided by spin-exchange in a partially fluorinated steroid (Scheme 2). Spin diffusion has been monitored[9,10] using spin-exchange spectroscopy based on an EXSY experiment (Figure 22). The rate of spin diffusion between protons is governed by the distance-dependent dipolar coupling only. Spin-diffusion between fluorine nuclei is also determined by the dipolar coupling. However, it can in addition be influenced by the spectral separation. In that case the elementary step in spin diffusion, the flip-flop between two coupled spins is no longer energy conserving. This has been investigated at moderate sample spinning rates with variations in the mixing time. Such moderate MAS rates, in conjunction with heteronuclear decoupling, provide sufficient line narrowing for the detection of highly resolved spectra. The heteronuclear coupling in this system is still significant at these spinning speeds. Therefore it is possible to effectively manipulate the dipolar coupling by RF pulses, e.g., during the mixing time, so as to investigate the various factors influencing fluorine spin diffusion. When no radio-frequency pulses are applied during mixing (Figure 22a), the spin-exchange rate reflects the spatial proximity of the fluorine nuclei in the molecule. If, however, the proton–fluorine dipolar coupling is suppressed during the EXSY mixing time, no exchange cross-peaks are visible between the CF and the CFH or the CFH_2 fluorine signals (Figure 22b) because suppression of the heteronuclear coupling leads to line narrowing, giving well-resolved, isolated lines in the spectrum. The spin-exchange process is no longer energy conserving and so is hindered. The opposite is true when the chemical shift difference is refocused and the line narrowing by MAS is stopped by rotor-synchronized π pulses during the mixing time (radio-frequency driven recoupling, RFDR). In such experiments (Figure 22c) the exchange rates are determined by the dipolar coupling strength and thus the internuclear distance only. In the case of RFDR, the exchange rate reflects the internuclear distance only when the chemical shift difference in the spectrum is refocused. Spin exchange is nearly suppressed when heteronuclear decoupling is applied. In the fully coupled spectra the exchange rate is influenced by the partial separation of the lines.

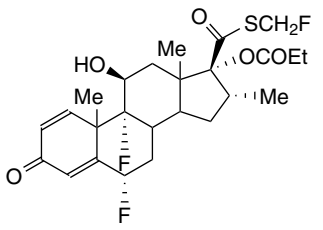

Scheme 2

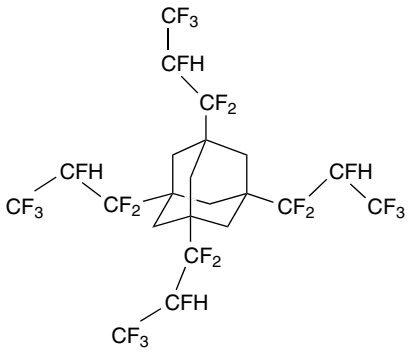

Scheme 3

The cross-polarization and relaxation behavior has been investigated[9,64] in a semifluorinated derivative of adamantane (Scheme 3). This molecule contains four identical sidechains

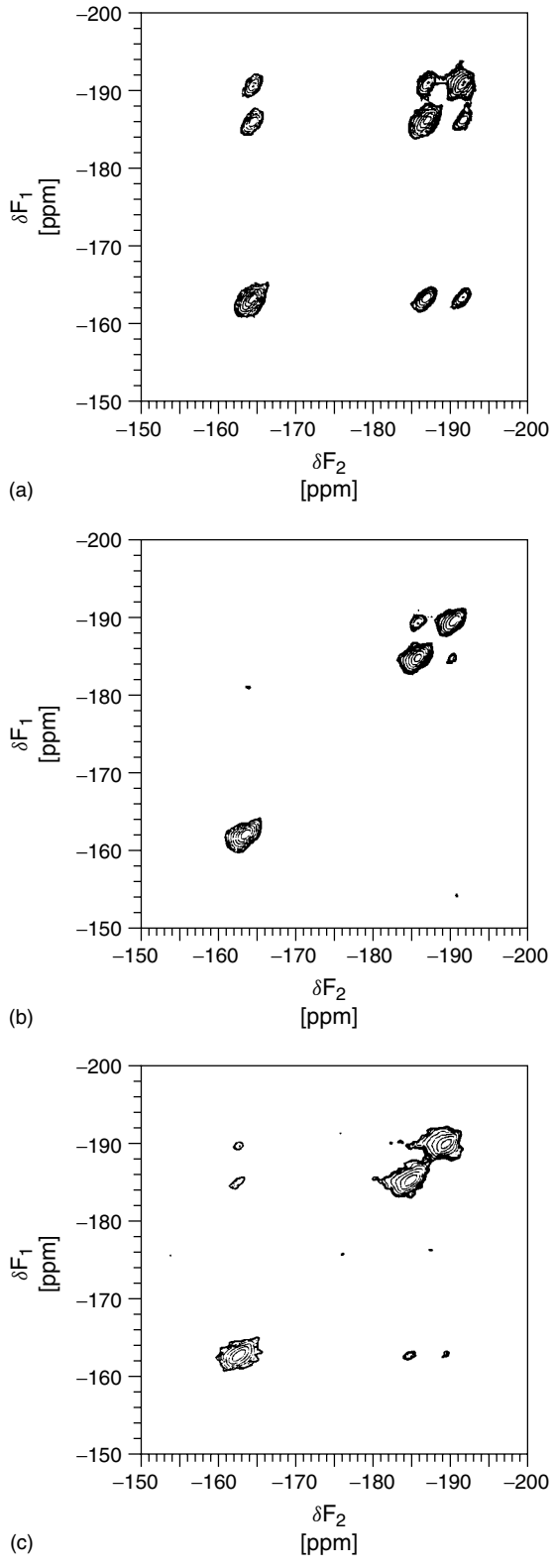

Figure 22 Two-dimensional 188.29 MHz ^{19}F CPMAS spin-exchange spectra of the fluorosteroid (Scheme 2): (a) without proton decoupling during the mixing time; (b) with proton decoupling during the mixing time; and (c) with RFDR during the mixing time. In all three cases the dwell time in both dimensions was 50 μs, the mixing time 5 ms, spinning rate 10 kHz, recycle delay 2 s, $\pi/2$ pulse duration 3 μs, contact time 2 ms, 32 transients per t_1 point and 128 slices in t_1

containing a CF_2, a CFH and a CF_3 group each. Different experimental methods for probing the dipolar coupling have been applied. By application of a variant of the DIPSHIFT experiment,[65] the heteronuclear dipolar coupling has been correlated with the fluorine chemical shift. Complementary information is obtained from a WISE (wideline separation experiment), where proton wideline information is correlated with the chemical shift of the neighboring fluorine nuclei. Both experiments can be utilized to probe local dynamics, which, via fluorine chemical shifts, can be attributed to chemical substructures. One-dimensional versions of the experiments, on the other hand, can be used as discriminating steps.

Brouwer et al.[66] have examined the supramolecular inclusion compound *p-tert* -butylcalix[4]arene-fluorobenzene, using $^1H \rightarrow {}^{19}F$ cross-polarization spectra to show that there must be considerable mobility of the guest fluorobenzene molecule in the host. Spectra of the static complex showed axially symmetric powder patterns with shielding anisotropy $\Delta\sigma = -42$ ppm, whereas solid fluorobenzene has an asymmetric shielding tensor[67] with $\Delta\sigma = -87$ ppm. The results[66] for the calixarene host-guest system are consistent with disorder in the crystal structure. Brouwer, Challoner and Harris[68] have studied a second *p-tert*-butylcalix[4]arene inclusion compound, with α, α, α-trifluorotoluene as a guest. The static $^{19}F-\{^1H\}$ spectra were analyzed (Figure 23) in terms of interplay between shielding anisotropy and F,F dipolar coupling to yield the 3 principal components of the shielding tensor and the F,F distances within the CF_3 group. Both shielding and dipolar tensors are strongly averaged by internal rotation about the $C-CF_3$ bond. The authors also studied the effect of magic-angle and off-angle spinning. The ^{19}F signal is narrow and very sensitive to the exact angle of the spinning axis. It is therefore proposed[68] that the compound be used to set the magic angle for ^{19}F spectra when proton decoupling is feasible.

Chisholm et al.[69] examined the $^{19}F-\{^1H\}$ MAS spectra of two monofluorinated pigment compounds and showed that in each case there is only one molecule in the asymmetric unit. Campbell et al.[70] examined two polymorphs of (3*S-trans*)-1-[3,4-dihydro-2,2-dimethyl-6-(pentafluoroethyl)-2*H*-1-benzo-pyran-4-yl]piperidin-2-one but found, somewhat unusually, that the $^1H \rightarrow {}^{19}F$ CP spectra did not distinguish very clearly between the forms, even though one (only) of them had more than one molecule in the crystallographic asymmetric unit. The ^{13}C spectra proved to be significantly more useful than the ^{19}F spectra.

Shapiro et al.[71] have shown that ^{19}F MAS NMR without proton decoupling gives high-resolution spectra for studying organic solid-phase reaction processes occurring on resin supports, using solvent-swelling (with benzene-d_6) to further decrease the linewidths. Specifically, they studied the reaction of 4-fluoro-3-nitrobenzamide, bonded to a polystyrene resin, with reagents causing an S_NAr displacement of the fluorine atom. The technique is complementary to gel-phase NMR and has the advantage of requiring less accumulation time. Grage et al.[72] applied a CPMG sequence to obtain pure dipolar spectra of flufenamic acid in a membrane (DMPC; 1,2-dimyristoyl-sn-glycero-3-phosphocholine) and, earlier,[73] diflucortolon-21-valerate in a fluorine-19-labelled DMPC; [1-myristoyl-2-(4,4-difluoro-

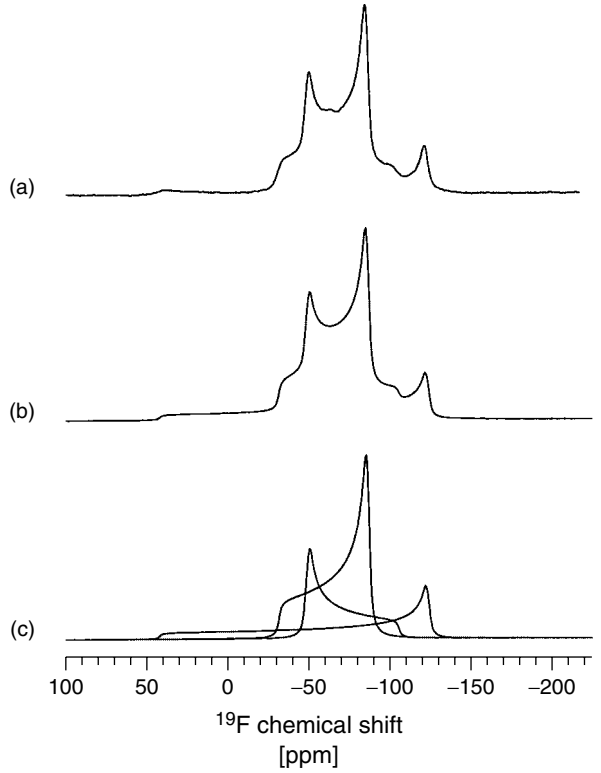

Figure 23 Experimental (a) and simulated (b) 188.297 MHz $^{1}H \rightarrow {}^{19}F\{H\}$ static NMR spectra of the *p-tert*-butylcalix[4]arene-α, α, α-trifluorotoluene inclusion compound. The three spectral components are depicted in (c). (Reproduced with permission from Ref.[68])

myristoyl)-sn-glycero-3-phosphocholine (DMPC-F_2)]. An investigation of the orientation dependence of the dipolar coupling strength in oriented membranes yields an order parameter. However, the axial rotation of the lipid molecules, which scales the dipolar couplings, has to be taken into account. With a two-dimensional version of the CPMG experiment, in which for each datapoint a full FID has been acquired, fluorine chemical shift resolution has been achieved under proton decoupling. A further report[74] on flufenamic acid in DMPC (but with the membrane named as dimyristoylphosphatidylcholine) was published by the same group later. In all three papers a range of NMR experiments (including Hahn echoes, CPMG pulse trains, and single-pulse excitation) was used, on static samples.

6 FLUORINATED ORGANOMETALLIC AND METAL COORDINATION COMPOUNDS

Surprisingly little work has been carried out in this area. Harris and co-workers[9,75] have used $^{19}F-\{^{1}H\}$ MAS NMR to study some organotin fluorides, R_3SnF. Spinning sideband analysis was carried out both on the main signals (arising from molecules containing spin-zero tin isotopes) and on the '$^{117/119}$Sn satellites' (Figure 24). Together with similar measurements on the $^{119}Sn-\{^{1}H\}$ spectra, the results enabled the authors to estimate the anisotropies in $^{1}J_{SnF}$, though with very large potential errors. In the case of Mes_3SnF (where Mes = mesityl) there are two molecules (with tetracoordinated

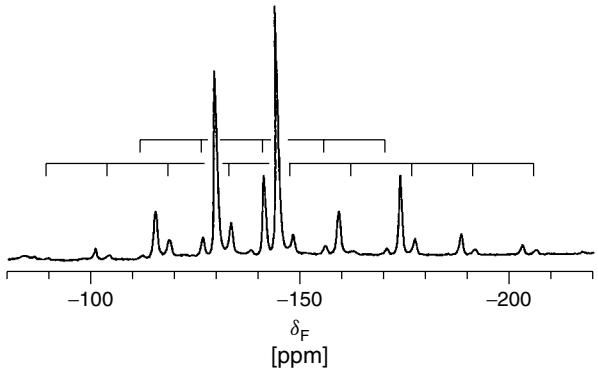

Figure 24 188.29 MHz fluorine-19 MAS spectrum of tri-*iso*butyltin fluoride, with the spinning sideband manifolds of the two 'tin satellite' resonances indicated separately. Experimental conditions: $\pi/2$ pulse duration 3.95 μs, spinning rate 2.7 kHz, 128 transients and 5 s recycle delay

tin) in the asymmetric unit and two-dimensional ^{119}Sn, ^{19}F HETCOR spectra enabled the ^{119}Sn and ^{19}F signals to be linked. The experiment was carried out with proton decoupling on both channels. The compound $^{n}Bu_3SnF$, on the other hand, contains pentacoordinate tin (involving Sn–F–Sn bridges), and the ^{19}F shielding anisotropy is substantially larger than for Mes_3SnF.

7 FLUORINATED INORGANIC COMPOUNDS

$^{1}H \rightarrow {}^{19}F$ cross-polarization and direct-polarization MAS spectra (along with ^{13}C and ^{31}P) have been obtained[76] for a solid chlorophosphane with aryl groups containing CF_3 substituents. Four signals were resolved throughout the temperature range −120 °C to +50 °C showing that local symmetry for the 2,6-$(CF_3)_2C_6H_3$ aromatic ring is lacking and that internal rotation about the relevant P–C bond is slow (which is not the situation in solution above ambient probe temperature). In contrast, the $^{19}F-\{^{1}H\}$ solid-state spectrum of a compound containing the 2,6-$(CF_3)_2C_6H_3PCl_2$ group as a ligand bonded to platinum shows[77] a single centreband signal at ambient temperature but a marked change to a more complex spectrum at low temperature. This suggests the slowing of a motional process (either rotation about the C–P bond or about the C–CF_3 bonds) as the temperature is lowered.

Fluorinated diazadiphosphetidines have been studied[78] by variable-temperature $^{19}F-\{^{1}H\}$ direct-polarization spectroscopy. At room temperature the fluorines in $(F_3PNPh)_2$ are all equivalent because of the existence of a rapid pseudorotation process. However, it was shown that at −106 °C this motion becomes slow on the NMR timescale.

8 CONCLUDING REMARKS

It is now clear that ^{19}F NMR has considerable potential for the study of molecular-level mobility and structure of solids across a wide range of chemistry. This is true for heterogeneous systems such as fluoropolymers, as well as for crystalline molecular and framework compounds, including biochemical situations. The considerable benefits from the

high natural abundance, strong magnetic dipole moment and substantial range of isotropic chemical shifts can now be routinely utilized because the technical problems of obtaining high-resolution ^{19}F spectra of excellent quality have now been overcome.

9 REFERENCES

1. R. K. Harris and P. Jackson, *Chem. Rev.*, 1991, **91**, 1427.
2. J. M. Miller, *Prog. NMR Spectrosc.*, 1996, **28**, 255.
3. V. J. McBrierty and K. J. Packer, 'Nuclear Magnetic Resonance in Solid Polymers', Cambridge University Press: Cambridge, 1993.
4. A. M. Kenwright and B. J. Say, in 'NMR Spectroscopy of Polymers', ed R. N. Ibben, Chapter 7, Chapman and Hall: London, 1993.
5. V. J. McBrierty and D. C. Douglass, *Macromolecules*, 1977, **10**, 855.
6. J. Schaefer and E. O. Stejskal, *J. Am. Chem. Soc.*, 1976, **98**, 1031.
7. E. W. Hagaman, *J. Magn. Reson.*, 1993, **104A**, 125.
8. S. A. Carss, R. K. Harris, P. Holstein, B. J. Say, and R. A. Fletton, *J. C. S. Chem. Commun.*, 1994, 2407.
9. R. K. Harris, S. A. Carss, R. D. Chambers, P. Holstein, A. P. Minoja, and U. Scheler, *Bull. Magn. Reson.*, 1995, **17**, 37.
10. S. A. Carss, U. Scheler, R. K. Harris, P. Holstein, and R. A. Fletton, *Magn. Reson. Chem.*, 1996, **34**, 63.
11. S. A. Vierkötter, *J. Magn. Reson.*, 1996, **118A**, 84.
12. B. C. Gerstein, R. G. Pembleton, R. C. Wilson, and L. M. Ryan, *J. Chem. Phys.*, 1977, **66**, 361.
13. S. F. Dec, R. A. Wind, G. E. Maciel, and F. E. Anthonio, *J. Magn. Reson.*, 1986, **70**, 355.
14. P. K. Isbester, T. A. Kestner, and E. J. Munson, *Macromolecules*, 1997, **30**, 2800.
15. U. Scheler, *Bull. Magn. Reson.*, 1999, **19**, 52.
16. R. D. Kendrick and C. S. Yannoni, *J. Magn. Reson.*, 1987, **75**, 506.
17. W. S. Veeman and W. E. J. R. Maas, *NMR Basic Principles Prog.*, 1994, **32**, 127.
18. P. van Hecke, H. W. Spiess, and U. Haeberlen, *J. Magn. Reson*, 1976, **22**, 103–116.
19. U. Scheler and R. K. Harris, *Chem. Phys. Lett.*, 1996, **262**, 137.
20. A. D. Bax, *J. Magn. Reson.*, 1985, **65**, 142–145.
21. (a) N. Zumbulyadis, *Phys. Rev.*, 1986, **33B**, 6495; (b) K. Schmidt-Rohr, J. Claus, and H. W. Spiess, *Macromolecules*, 1992, **25**, 3273.
22. U. Scheler and R. K. Harris, *Solid State NMR*, 1996, **7**, 11.
23. E. Brunner, D. Freude, B. C. Gerstein, and H. Pfeifer, *J. Magn. Reson.*, 1990, **90**, 90.
24. P. Holstein, R. K. Harris, and B. J. Say, *Solid State NMR*, 1997, **8**, 201.
25. P. Holstein, U. Scheler, and R. K. Harris, *Polymer*, 1998, **39**, 4937.
26. S. Ando, R. K. Harris, P. Holstein, S. A. Reinsberg, and K. Yamauchi, *Polymer*, 2001, **42**, 8137.
27. P. Holstein, G. A. Monti, and R. K. Harris, *Phys. Chem. Chem. Phys.*, 1999, **1**, 3549.
28. M. Goldman and L. Shen, *Phys. Rev.*, 1966, **144**, 321.
29. L. Müller, A. Kumar, T. Baumann, and R. R. Ernst, *Phys. Rev. Lett.*, 1974, **32**, 1402.
30. S. A. Reinsberg, S. Ando, and R. K. Harris, *Polymer*, 2000, **41**, 3729.
31. M. Lee and W. I. Goldburg, *Phys. Rev.*, 1965, **140A**, 1261.
32. S. R. Hartmann and E. L. Hahn, *Phys. Rev.*, 1962, **128**, 2042–2053.
33. B.-J. van Rossum, C. P. de Groot, V. Ladizhansky, S. Vega, and H. J. M. de Groot, *J. Am. Chem. Soc.*, 2000, **1222**, 3465.
34. T. Miyoshi and U. Scheler, to be published.
35. T. Miyoshi and U. Scheler, *Solid State NMR*, in preparation.
36. D. A. McArthur, E. L. Hahn, and R. E. Walstedt, *Phys. Rev.*, 1969, **188**, 609–638.
37. M. Mehring, 'Principles of High Resolution NMR in Solids', 'NMR – Basic Principles and Progress', 2nd edn., Vol. 11. Spinger: Berlin 1983.
38. D. Michel and F. Engelke, *NMR Basic Principles Prog.*, 1994, **32**, 69.
39. S. Ando, R. K. Harris, and S. A. Reinsberg, *J. Magn. Reson.*, 1999, **141**, 91.
40. S. Ando, R. K. Harris, G. A. Monti, and S. A. Reinsberg, *Magn. Reson. Chem.*, 1999, **37**, 709.
41. P. Tekely, V. Gerardy, P. Palmas, D. Canet, and A. Retournard, *Solid State NMR*, 1995, **4**, 361.
42. P. Hazendonk, R. K. Harris, G. Galli, and S. Pizzanelli, *Phys. Chem. Chem. Phys.*, 2002, **4**, 507.
43. R. K. Harris, G. A. Monti, and P. Holstein, 'Solid State NMR of Polymers.', eds I. Ando and T. Asakura, Elsevier Science: New York, 1998, ch 6.6, pp 253–266.
44. R. K. Harris, G. A. Monti, and P. Holstein, 'Solid State NMR of Polymers', eds I. Ando and T. Asakura, Elsevier Science: New York, 1998, ch 18, pp 667–712.
45. P. K. Isbester, J. L. Brandt, T. A. Kestner, and E. J. Munson, *Macromolecules*, 1998, **31**, 8192.
46. R. K. Harris, R. R. Yeung, P. Johncock, and D. A. Jones, *Polymer*, 1996, **37**, 721.
47. G. A. Monti and R. K. Harris, *Magn. Reson. Chem.*, 1998, **36**, 892.
48. T-.W. Su and D-.L. M. Tzou, *Polymer*, 2000, **41**, 7289.
49. S. Ando, R. K. Harris, and S. A. Reinsberg, *Magn. Reson. Chem.*, 2002, **40**, 97.
50. P.-Y. Mabboux and K. K. Gleason, *J. Fluorine Chem.*, 2002, **113**, 27.
51. K. K. S. Lau and K. K. Gleason, *J. Electrochem. Soc.*, 1999, **146**, 2652.
52. K. K. S. Lau and K. K. Gleason, *J. Fluorine Chem.*, 2000, **104**, 119.
53. W. H. Press, B. F. Flannery, S. A. Teukolsky, and W. T. Vetterling, 'Numerical Recipes: The Art of Science Computing', Cambridge University Press: Cambridge, 1987, ch 14, pp 523.
54. S. A. Carss, Ph.D. Thesis, University of Durham, 1995.
55. A. Nordon, R. K. Harris, L. Yeo, and K. D. M. Harris, *J. C. S. Chem. Commun.*, 1997, 961.
56. A. Nordon, Ph.D. Thesis, University of Durham, 1997.
57. A. Nordon, E. Hughes, R. K. Harris, L. Yeo, and K. D. M. Harris, *Chem. Phys. Lett.*, 1998, **298**, 25.
58. R. K. Harris, A. Nordon, and K. D. M. Harris, *Magn. Reson. Chem.*, 1999, **37**, 15.
59. R. K. Harris, 'Magnetic Resonance in Food Science: A View to the Future', eds G. A. Webb, P. S. Belton, A. M. Gil, and I. Delgadillo, Royal Society of Chemistry: London, 2001, ch. 3.
60. A. E. Bennett, J. H. Ok, and R. G. Griffin, *J. Chem. Phys.*, 1992, **96**, 8624.
61. I. Schnell, S. P. Brown, H. Y. Low, H. Ishida, and H. W. Spiess, *J. Am. Chem. Soc.*, 1998, **120**, 11 784.
62. U. Scheler, *Prog. NMR Spectrosc.*, in preparation.
63. B. Fuchs and U. Scheler, *Macromolecules*, 2000, **33**, 120.
64. R. K. Harris and U. Scheler, to be published.
65. M. G. Munowitz and R. G. Griffin, *J. Chem. Phys.*, 1982, **76**, 2848.
66. E. B. Brouwer, R. D. M. Gougeon, J. Hirschinger, K. A. Udachin, R. K. Harris, and J. A. Ripmeester, *Phys. Chem. Chem. Phys.*, 1999, **1**, 4043.
67. a. M. Mehring, H. Raber, and G. Sinning, *Proc. Congr. Ampére, 18th*, 1974, **1**, 35. b. U. Haeberlen, *Adv. Magn. Reson. Suppl.*, 1976, **1**, 142.
68. E. B. Brouwer, R. Challoner, and R. K. Harris, *Solid State NMR*, 2000, **18**, 37.

69. G. Chisholm, B. Hay, K. D. M. Harris, S. J. Kitchin, and K. M. Morgan, *Dyes & Pigments*, 1999, **42**, 159.
70. S. C. Campbell, R. K. Harris, M. J. Hardy, D. C. Lee, and D. J. Bushby, *J. Chem. Soc. Perkin Trans 2*, 1997, 1913.
71. M. J. Shapiro, G. Kumaravel, R. C. Petter, and R. Beveridge, *Tetrahedron Lett.*, 1996, **37**, 4671.
72. S. L. Grage and A. S. Ulrich, *J. Magn. Reson.*, 2000, **146**, 81.
73. S. L. Grage and A. S. Ulrich, *J. Magn. Reson.*, 1999, **138**, 98.
74. S. L. Grage, D. R. Gauger, C. Selle, W. Pohle, W. Richter, and A. S. Ulrich, *Phys. Chem. Chem Phys.*, 2000, **2**, 4574.
75. J. C. Cherryman and R. K. Harris, *J. Magn. Reson.*, 1997, **128**, 21.
76. A. S. Batsanov, S. M. Cornet, L. A. Crowe, K. B. Dillon, R. K. Harris, P. Hazendonk, and M. D. Roden, *Eur. J. Inorg. Chem.*, 2001, 1729.
77. (a) L. A. Crowe, K. B. Dillon, R. K. Harris, J. A. K. Howard, and M. D. Roden, to be published; (b) L. A. Crowe, Ph.D. Thesis, University of Durham, 2000.
78. R. K. Harris and L. A. Crowe, *J. Chem. Soc. Dalton*, 1999, 4315.

Acknowledgements

R. K. H. thanks the U.K. Engineering and Physical Sciences Research Council, which provided finances for the purchase of a spectrometer (research grant GR/J97557) and for staff (research grants GR/L02906 and GR/M73514). We are grateful to Dr. Paul Hazendonk for preliminary information on copoly. U.S. thanks the IPF for continuous support and the Deutsche Forschungsgemeinshaft for a fellowship (SCHE 524/1-1).

Biographical Sketches

Shinji Ando, *b* 1960. B.Eng., 1984, M.Eng.,1986, and Ph.D 1989, Tokyo Institute of Technology. Research Scientist at Nippon Telegraph and Telephone Corporation, 1989–1995. Associate Professor of the Department of Organic and Polymeric Materials at Tokyo Institute of Technology, 1995–present. Visiting Scientist of the Department of Chemistry, University of Durham, UK, 1998–1999. Research interests include characterization of fully aromatic polymers and fluoropolymers using solid-state NMR and optical spectroscopies.

Robin K. Harris, *b* 1936. B.A. (Nat. Sci.), Ph.D., (supervisor Norman Sheppard), Sc.D., University of Cambridge, UK. Postdoctoral work at Mellon Institute, Pittsburgh, PA (with Aksel Bothner-By). Successively lecturer, senior lecturer, and professor, University of East Anglia, UK. Currently Professor of Chemistry, University of Durham, UK. Secretary-General of ISMAR, 1986–92. Approx. 450 publications. Current research specialty: solid-state NMR and its applications in materials chemistry.

Ulrich Scheler, *b* 1964. Diploma in Physics 1991, Technical University of Dresden. Research student in the Max-Planck Institute for Polymer Research, Mainz (with H. W. Spiess), Ph.D. awarded 1994, University of Mainz. Postdoctoral Fellow, Department of Chemistry, University of Durham, U.K. (with R. K. Harris) 1994–1996. 1996–present: Institute for Polymer Research, Dresden, Germany, (1997–2000 fellowship from Deutsche Forschungsgemeinschaft, DFG). Currently head of the Surface Modification Department. Current Research interests: solid-state NMR based on high-speed MAS with a focus on ^{19}F, $^{1}H-^{19}F$ and $^{1}H-^{19}F$–X NMR, fluoropolymers, polyelectrolytes, diffusion and electrophoresis NMR.